Biophysical Journal Volume 107 November 2014 2274–2286

Article

Area per Lipid and Cholesterol Interactions in Membranes from Separated Local-Field ^{13}C NMR Spectroscopy

Avigdor Leftin,[1] Trivikram R. Molugu,[1] Constantin Job,[1] Klaus Beyer,[1] and Michael F. Brown[1,2,*]
[1]Department of Chemistry and Biochemistry and [2]Department of Physics, University of Arizona, Tucson, Arizona

ABSTRACT Investigations of lipid membranes using NMR spectroscopy generally require isotopic labeling, often precluding structural studies of complex lipid systems. Solid-state ^{13}C magic-angle spinning NMR spectroscopy at natural isotopic abundance gives site-specific structural information that can aid in the characterization of complex biomembranes. Using the separated local-field experiment DROSS, we resolved ^{13}C-^{1}H residual dipolar couplings that were interpreted with a statistical mean-torque model. Liquid-disordered and liquid-ordered phases were characterized according to membrane thickness and average cross-sectional area per lipid. Knowledge of such structural parameters is vital for molecular dynamics simulations, and provides information about the balance of forces in membrane lipid bilayers. Experiments were conducted with both phosphatidylcholine (dimyristoylphosphatidylcholine (DMPC) and palmitoyloleoylphosphatidylcholine (POPC)) and egg-yolk sphingomyelin (EYSM) lipids, and allowed us to extract segmental order parameters from the ^{13}C-^{1}H residual dipolar couplings. Order parameters were used to calculate membrane structural quantities, including the area per lipid and bilayer thickness. Relative to POPC, EYSM is more ordered in the l_d phase and experiences less structural perturbation upon adding 50% cholesterol to form the l_o phase. The loss of configurational entropy is smaller for EYSM than for POPC, thus favoring its interaction with cholesterol in raftlike lipid systems. Our studies show that solid-state ^{13}C NMR spectroscopy is applicable to investigations of complex lipids and makes it possible to obtain structural parameters for biomembrane systems where isotope labeling may be prohibitive.

INTRODUCTION

Lipid-protein interactions (1) and the associated functions of biomembranes (2–6) are known to be significantly influenced by the composition (2,7–11) and structure of the lipid bilayer (6,11–16). Recently, the importance of lipids in cellular membranes and tissues has made lipidomics (17) an emerging field in biomedical research. Essential roles of membrane lipids are brought out by the sphingolipids, which are implicated in human disorders including Tay-Sachs, Niemann-Pick, Gaucher (18), Parkinson's (19), and Huntington diseases (20). Sphingolipids are attracting much attention to so-called lipid rafts in cellular membranes (4,9,21–27). Moreover, in vitro studies of integral membrane proteins or peptides often require that they be reconstituted with membrane lipids (19,28–30), where bilayer structural dimensions involving hydrophobic matching and area per lipid are significant factors (1,14,31). The constraints imposed by the area per lipid at the membrane aqueous interface (31) also play an important part in validating molecular dynamics (MD) simulations of lipid bilayers (32) and biomembranes (13,33,34). In such cases, it is essential that investigators have a solid understanding of the membrane bilayer structure itself (35).

Despite advances in technology (19,36–45), there is an enduring thirst for new methods on account of the strengths and limitations inherent in existing biophysical techniques. This work is aimed at extending such investigations by using for the first time to our knowledge a combination of separated local-field (SLF) NMR spectroscopy (41,46–48) and statistical mean-torque theory (35). Studies of natural lipids, as well as natural detergents (49), can benefit from extending methods originally developed for ^{2}H NMR spectroscopy (50) to cases where ^{2}H-isotope labeling is impractical. Simple geometrical observations are the basis of a mean-field model used for analysis of both small-angle x-ray scattering (SAXS) and solid-state ^{2}H NMR data (51). The first-order mean-torque model (35) evaluates the average cross-sectional area and volumetric hydrocarbon thickness of the membrane lipids. For multicomponent membranes, the ensemble structures derived from the repeat spacings or electron densities in SAXS do not resolve the contributions from individual lipid species. However, average cross-sectional areas for multicomponent lipid mixtures are obtainable from residual quadrupolar couplings in solid-state ^{2}H NMR spectroscopy, which typically requires isotopically labeled lipids for each component studied (52).

Here, we demonstrate the applicability of mean-field modeling of membrane structure in conjunction with a solid-state ^{13}C NMR technique that does not require isotopic enrichment. Magic-angle spinning (MAS) NMR resolves site-specific details for individual lipid species in

Submitted February 11, 2014, and accepted for publication July 15, 2014.
*Correspondence: mfbrown@u.arizona.edu
Avigdor Leftin and Trivikram R. Molugu contributed equally to this work.
Avigdor Leftin's present address is Department of Chemical Physics, Weizmann Institute of Science, Rehovot 76100, Israel.
Editor: Klaus Gawrisch.

0006-3495/14/11/2274/13 $2.00
http://dx.doi.org/10.1016/j.bpj.2014.07.044

membranes (28,47,53–56), thus enabling a range of biologically significant applications. We show how the steric hydrocarbon thickness and average cross-sectional areas are derived from solid-state ^{13}C-^{1}H residual dipolar couplings (RDCs) for sphingolipids and phospholipids in single-component and cholesterol-enriched binary mixtures. Two-dimensional (2D) solid-state ^{13}C NMR spectroscopy (46) can probe the headgroup, backbone, and acyl chain regions for membrane components simultaneously, including cholesterol at natural isotopic abundance (19,46,57). In addition, the membrane phase behavior is further quantified, giving a valuable probe of lipid interactions in bilayers, as well as in natural biomembranes.

MATERIALS AND METHODS

Preparation of multilamellar lipid dispersions

1,2-dimyristoyl-*sn*-glycero-3-phosphocholine (DMPC), 1-palmitoyl-2-oleoyl-*sn*-glycero-3-phosphocholine (POPC), and egg yolk sphingomyelin (EYSM) (predominant species *N*-(palmitoyl)-sphing-4-enine-1-phosphocholine) were procured from Avanti Polar Lipids (Alabaster, AL), and cholesterol (chol) was from Sigma-Aldrich (St. Louis, MO). The lipids were dissolved in hexane and lyophilized to yield dry powders. Multilamellar lipid dispersions were prepared by hydrating the dry lipid powders with 50 wt % deuterium oxide (Cambridge Isotopes, Cambridge, MA). These dispersions were subjected to three to five freeze-thaw mixing cycles to ensure homogeneity. Samples were tested for ester hydrolysis before and after the experiments using thin-layer chromatography (TLC) by elution with $CHCl_3$/MeOH/H_2O (65:30:5), followed by charring with 40% H_2SO_4 in ethanol.

Implementation of DROSS experiments

Separated local-field ^{13}C MAS NMR experiments were conducted with a magnetic field strength of 11.7 T (500 MHz ^{1}H Larmor frequency) using a Bruker AVANCE-I spectrometer system. The SLF experiment, involving dipolar recoupling on-axis with scaling and shape preservation (DROSS) (46), was implemented on the Bruker Topspin 2.1 software platform (Billerica, MA). A triple-channel MAS NMR probe (DSI-733) from Doty Scientific (Columbia, SC) was used for all experiments. Samples were contained in 4-mm zirconium rotors. Radiofrequency pulses for the ^{1}H and ^{13}C channels were adjusted to exactly the same duration, 3.5 μs for the 90° pulses. Dipolar recoupling at 6–8 kHz MAS frequency was achieved by applying four radiofrequency 180° pulses in one rotor period, with a chemical shift offset of $\varepsilon = 0$ and anisotropy scaling of $\chi_P = 0.393$ (46,58). The INEPT (insensitive nuclei enhanced by polarization transfer) buildup of anti-phase magnetization and refocusing delays was optimized empirically. The rotor-synchronized sampling of the indirect dimension (t_1) was achieved using the States method with a total of 64–128 points. The sampling of the direct time dimension (t_2) utilized 8192 points recorded with an interval of 10 μs with 50-kHz ^{1}H SPINAL-32 decoupling (59). Recycle times were 3 s, and between 1000 and 2000 transients were averaged for each t_2 record, giving total experiment times ranging from 24–48 h. The fluctuations in rotor spinning speed were controlled to ±2 Hz with a Doty Scientific spin-rate controller. Sample temperature was controlled using a Bruker variable temperature unit and is accurate to ±1°C. The reported ^{13}C NMR chemical shifts were referenced to TMS (external).

Fourier transformation of the t_1 and t_2 dimensions was carried out and analyzed using the Bruker Topspin software. A 10-Hz Lorentzian broadening was applied in the t_2 dimension, and a 50- to 250-Hz Gaussian apodization was applied in the t_1 dimension after zero-filling to 128–256 points.

Fits to ^{13}C SLF DROSS magnetic dipolar lineshapes were generated using the Topspin solid lineshape analysis (SOLA) software and verified using standard algorithms for the Pake lineshape coded in Matlab (Natick, MA). Segmental order parameters are defined as (50)

$$S_{CH} = \frac{1}{2}\langle 3\cos^2\beta_{CH} - 1\rangle, \quad (1)$$

where β_{CH} is the instantaneous angle between the ^{13}C-^{1}H bond direction and the bilayer normal. Based on geometrical considerations, the S_{CH} order parameters for a polymethylene chain are negative.

Here, we refer to the absolute order parameters $|S_{CH}|$, calculated from the relation

$$|S_{CH}| = \frac{|\Delta\nu_D|}{\chi_D\chi_P}. \quad (2)$$

In the above formula, $\chi_D = (-\mu_0\gamma_H\gamma_C\hbar/4\pi^2)\langle r^{-3}\rangle$ is the dipolar coupling constant (40.783 kHz corresponding to $b_{CH}/2\pi = 20.392$ kHz) for an aliphatic ^{13}C-^{1}H bond (46), $\chi_P = 0.393$ is the pulse-sequence scaling factor (46), and $\Delta\nu_D$ is the measured RDC evaluated at the $\theta = 90°$ orientation of the lineshape (Pake powder pattern). The estimated random error of the RDCs is ≈ ±4%, corresponding to a ±4% error of the segmental order parameters. Possible sources of systematic errors include the value of the rigid-lattice (static) dipolar coupling constant as well as the chemical-shift assignments. Note that the above dipolar coupling constant corresponds to an effective equilibrium internuclear ^{13}C-^{1}H distance of $\langle r^{-3}\rangle^{-1/3} = 1.14$ Å due to the correction for dynamic effects, as first shown in our previous work (60). For resonance assignments of the ^{13}C isotropic chemical-shift spectra, ChemBioDraw (PerkinElmer, Waltham, MA)-based simulations based on additivity relations for isotropic liquids (61–65) were initially used. However, because the chemical shifts due to liquid-crystalline phase conformations are not averaged to their isotropic values, we introduced ^{2}H NMR-derived $|S_{CD}|$ order-parameter-based peak assignments (43). In this article, we compare the calculated $|S_{CH}|$ order parameter values with $|S_{CD}|$ order parameters used for the peak assignments. Such methods are helpful in identifying the ^{13}C resonance peaks coming from the hydrocarbon chains of the liquid-crystalline phospholipids.

Theoretical Framework of Mean-Torque Model

For membrane lipids, the dipolar or quadrupolar couplings are reduced from their rigid-lattice (static) values due to segmental and molecular motions as well as collective fluctuations of the entire bilayer (66). The various motions are described by their mean-squared amplitudes and (reduced) spectral densities, and they may include cross correlations due to their statistical (in) dependence (66–68). The segmental order parameters (S_{CH} or S_{CD}) describe the composite motion in terms of the residual couplings (dipolar or quadrupolar) as compared to the static values (43). The order parameters are model-free spectroscopic observables that are statistical averages over all the motions, with correlation times up to the inverse of the rigid-lattice coupling (50). In analogy with liquid crystals, each segment is considered independently, because the spectroscopic observables are site-specific (50,69). Correlations among the motions along the chains and between the chains are included in the order parameters as a function of segmental position (35,70). Interpretation of the segmental order parameters in terms of lipid bilayer structure was first achieved using a diamond-lattice model (71,72). That model assumes discrete orientations of acyl chain segments as the most probable conformations. Although initially it appeared to be in reasonably good agreement with scattering experiments, discrepancies between the area calculations from more accurate ^{2}H NMR and x-ray scattering measurements became evident (73,74). The mean-torque model was proposed as an alternative (35), as it assumes a continuum distribution for the orientations of acyl chain segments. The mean-torque model successfully explains bilayer structural parameters for liquid-crystalline disaturated phospholipid membranes (35).

In this work, we introduce the applicability of the mean-torque model in connection with ^{13}C-NMR-derived segmental order parameters to interpret the membrane structure. Here, the main objective is connecting the lipid structural parameters to hydrocarbon-chain segmental order parameters. Changes due to osmotic stress or to headgroup and acyl chain composition are related to the balance of forces that govern membrane assembly and lipid-protein interactions (1). For disaturated lipids, a plateau is seen in the ^{2}H-NMR-derived segmental order parameter profile close to the headgroup. At a certain depth of the bilayer, the influence of chain terminations becomes important (75,76). Acyl chains on adjacent molecules become more disordered beyond this point to maintain the packing of hydrocarbon density (77). Another observation from ^{2}H NMR order profiles is that the plateau region shows a strong chain-length dependence, whereas nonplateau regions are practically independent of chain length (35). At the molecular scale, each lipid in the membrane occupies a space that on average is related to the volume and length of the hydrocarbon chains according to

$$D_C = \frac{2V_C}{\langle A\rangle}, \tag{3}$$

where D_C is the volumetric thickness of the hydrocarbon layer, and V_C is the total volume of an individual acyl chain. In Eq. 3, the volume, V_C, is assumed from the densitometry measurements of Nagle and co-workers (78) and is conserved (i.e., constant). Note that the volumetric thickness, D_C, and the mean area, $\langle A\rangle$, are inversely related by the assumption of constant volume, meaning that the bilayer core has approximately the density of liquid hydrocarbon (77,80). However, D_C is not the same as the mean projected acyl length, as discussed by Jansson et al. (79). Due to end effects of the acyl chains, the mean travel away from the aqueous interface is less than the distance to the bilayer midplane, as required for the well-established assumption of constant volume to apply (35). The chain volume at temperature T is found from the methylene volume, V_{CH_2}, using the expression $V_{CH_2} = V^0_{CH_2} + \alpha_{CH_2}(T - 273.15)$, where α_{CH_2} is the isobaric thermal expansion coefficient for methylene groups (35). It is well established that the volume of a methyl group is $V_{CH_3} \approx 2V_{CH_2}$ and that $V_{CH} \approx V_{CH_2}/1.31$ for the methine volume (78,80,81).

When the membrane composition is mixed, neighboring interactions between the lipids can lead to a change in the average cross-sectional area per lipid. To avoid complications from chain upturns (35,70), for estimating the average area per lipid instead of the area of the entire hydrocarbon chain, one can consider relatively ordered acyl segments near the headgroup region. For solid-state ^{13}C NMR (43) the largest RDC corresponds to the plateau region of the ^{2}H NMR order profiles, where it is reasonable to assume that the segmental cross-sectional area and projected length are inversely correlated, as discussed in Jansson et al. (79). The average cross-sectional area per lipid is thus given as (35)

$$\langle A\rangle = 4V_{CH_2}\left\langle\frac{1}{D}\right\rangle. \tag{4}$$

Here V_{CH_2} is the methylene volume (78) and D is the instantaneous travel of an individual segment along the bilayer normal. This expression can be further rewritten as

$$\langle A\rangle = \frac{4V_{CH_2}}{D_M}q, \tag{5}$$

where $D_M = 2.54$ Å is the maximum projection of the virtual bonds connecting every second carbon atom in the polymethylene chain to the bilayer normal, and $4V_{CH_2}/D_M$ is the lipid cross-sectional area of the extended all-*trans* conformation (35). The area factor q is defined as $\langle 1/\cos\beta\rangle^{-1}$, where β is the angle between the virtual bond axis connecting the C_{i-1} and C_{i+1} carbon atoms and the normal to the lipid bilayer surface.

In Eq. 5, Euclidean geometry is assumed by approximating the shape of a statistical segment by a geometrical prism with constant hydrocarbon volume (50). Consequently, the effective acyl segment length is averaged over the motions, whereas the segmental volume is not. As the motional amplitudes increase, so does the area per lipid, yet the volume per segment spanned in space remains approximately constant. It follows that a Taylor series expansion about the all-*trans* reference value allows the area factor q to be approximated by $q \approx 3 - 3\langle\cos\beta_i\rangle + \langle\cos^2\beta_i\rangle$ up to second order (35). For ^{13}C NMR, the second moment $\langle\cos^2\beta_i\rangle$ can be obtained directly from the absolute order parameters $|S^{(i)}_{CH}|$ of a given acyl segment (index i) by

$$\langle\cos^2\beta_i\rangle = \frac{1 + 4|S^{(i)}_{CH}|}{3}. \tag{6}$$

To interpret the $|S_{CH}|$ dipolar order parameters in terms of structural quantities, several models have been developed (35). Because of the inherent complexity of membrane structure, most of these models are confined to simplified statistical treatments of lipid conformations. Calculation of the first moment $\langle\cos\beta_i\rangle$ with a given value of $\langle\cos^2\beta_i\rangle$ is further described below.

The mean-torque model assumes that the orientational order for each chain segment relative to the local director is described by an orientational potential, $U(\beta)$ (potential of mean torque). With the combined effects of thermal fluctuations of the segmental orientations, both segmental and molecular conformations assume a continuous distribution. The probability of finding a statistical segment with a virtual bond orientation β ($\equiv \beta_{CH}$) at a given instant is given by the Boltzmann distribution,

$$f(\beta) = \frac{1}{Z}\exp\left(-\frac{U(\beta)}{k_BT}\right), \tag{7}$$

where the chain index i is also suppressed for clarity. Here, the partition function is

$$Z = \int_0^\pi \exp\left(-\frac{U(\beta)}{k_BT}\right)\sin\beta d\beta. \tag{8}$$

Assuming a first-order mean-torque model (35), the angle-dependent quantities are integrated with the distribution function to give the coupled equations

$$\langle\cos\beta\rangle = \coth\left(\frac{U(\beta)}{k_BT}\right) + \left(\frac{U(\beta)}{k_BT}\right)^{-1}; \tag{9}$$

$$\langle\cos^2\beta\rangle = 1 + 2\left(\frac{U(\beta)}{k_BT}\right)^{-2} - 2\left(\frac{U(\beta)}{k_BT}\right)^{-1}\coth\left(\frac{U(\beta)}{k_BT}\right). \tag{10}$$

An analytical solution for $\langle\cos\beta\rangle$ can then be obtained by using the approximation $\coth[U(\beta)/k_BT] \approx 1$, which for an individual segment (index i) yields the relation

$$\langle\cos\beta_i\rangle = \frac{1}{2}\left(1 + \sqrt{\frac{8|S^{(i)}_{CH}| - 1}{3}}\right). \tag{11}$$

It should be noted that for the all-*trans* conformation of the lipids, $\langle\cos\beta_i\rangle = \langle\cos^2\beta_i\rangle = 1$ and hence $q = 1$. It follows that Eqs. 3 and 4 give rise to a limiting area of $4V_{CH_2}/D_M$ and limiting monolayer thickness of $n_CD_M/2$, where n_C is the number of carbon atoms in the hydrocarbon chain.

Each molecule contributes to the average thickness for the lipid bilayer ensemble, which includes the headgroup plus backbone thickness in the sense of a Gibbs dividing surface. The volumetric (Luzzati) bilayer

thickness is $D_B = V_L/\langle A \rangle$ where V_L is the lipid volume (78) and $D_H = 4$ Å for DMPC or POPC and 6 Å for EYSM. Alternatively, an effective membrane bilayer thickness can be calculated using the expression,

$$D_B' = 2D_C + 2D_H, \quad (12)$$

where D_C is the volumetric hydrocarbon thickness of the two acyl chains of the lipid, and D_H is the headgroup plus the backbone distance. In the case of phospholipids, D_H is 9 Å, and for most sphingolipids it is 7 Å (82–84). Use of the above values of D_H and D_C corresponds to the steric bilayer thickness D_B' as defined by Nagle et al. (12). Finally, it is important to note that the first-order mean-torque model neglects the effects of collective slow motions (77). The above treatment of a mean-torque model was originally formulated in terms of ^{2}H NMR-derived S_{CD} values. However, we show equivalently that one can use S_{CH} order parameters obtained from natural-abundance ^{13}C NMR spectroscopy to extend the calculation of membrane structural parameters.

RESULTS

The INEPT-based SLF NMR experiment DROSS (46) was implemented for the two glycerophospholipids DMPC and POPC together with the sphingolipid EYSM and their binary mixtures with cholesterol. The DROSS experiment provides measurements for the headgroup, glycerol backbone, and acyl chain order parameters without isotopic enrichment. This is especially useful when comparing responses from these bilayer regions to changes in bilayer composition. However, accurate measurement of small absolute order parameters, as in the case of headgroup segments (85), is challenging in SLF spectroscopy. As an example, Fig. 1 shows a 2D SLF spectrum of a POPC/cholesterol (1:1) binary mixture at 30°C. The representative slices of the 2D DROSS spectrum shown in Fig. 1 *a* indicate that well-resolved RDCs (Pake doublets) are obtained. The RDCs can be used to obtain dipolar ^{13}C-^{1}H order parameters that are analogous to the C-^{2}H bond order parameters in solid-state ^{2}H NMR spectroscopy (50). An expansion of the 2D DROSS spectrum from the aliphatic fingerprint region is shown in Fig. 1 *b*. The slices parallel to the F_1 frequency axis for each of the chemically shifted (δ) resonances in the F_2 dimension give the site-specific RDCs (Pake doublets). Fig. 1 *c* shows a contour plot of the 2D DROSS spectrum together with the F_2 frequency projection corresponding to the 1D chemical-shift spectrum. A number of distinct ^{13}C resonances are observed due to the POPC acyl groups as well as cholesterol. Notably, the $(CH_2)_n$ envelope includes additional acyl chain resonances that are incompletely resolved due to inhomogeneous line broadening. They can be partially assigned by comparison to the results of solid-state ^{2}H NMR spectroscopy (see below). Further explanation of the SLF experiment is provided in Figs. S1–S4 in the Supporting Material.

Liquid-disordered phase of lipid bilayers

Our findings illustrate that SLF NMR spectroscopy is broadly applicable to a variety of synthetic and natural lipids. Fig. 2 *a* depicts a 2D plane of a DROSS spectrum for POPC in the liquid-crystalline state at 28°C. The F_2 frequency dimension (horizontal) shows the isotropic ^{13}C chemical shift (δ) spectra obtained under MAS. As mentioned above, the DROSS spectra contain Pake doublets corresponding to the ^{13}C-^{1}H dipolar couplings along the F_1 frequency axis (vertical). The dipolar slices correspond to each of the isotropic ^{13}C chemical-shift positions. A similar set of spectra representing EYSM at 48°C is shown in Fig. 2 *b*. Resonances from polar headgroups, glycerol backbone, and acyl chains of the lipids are clearly resolved. The ^{13}C chemical-shift assignments were taken from the literature (86,87) and were verified by simulations based on additivity

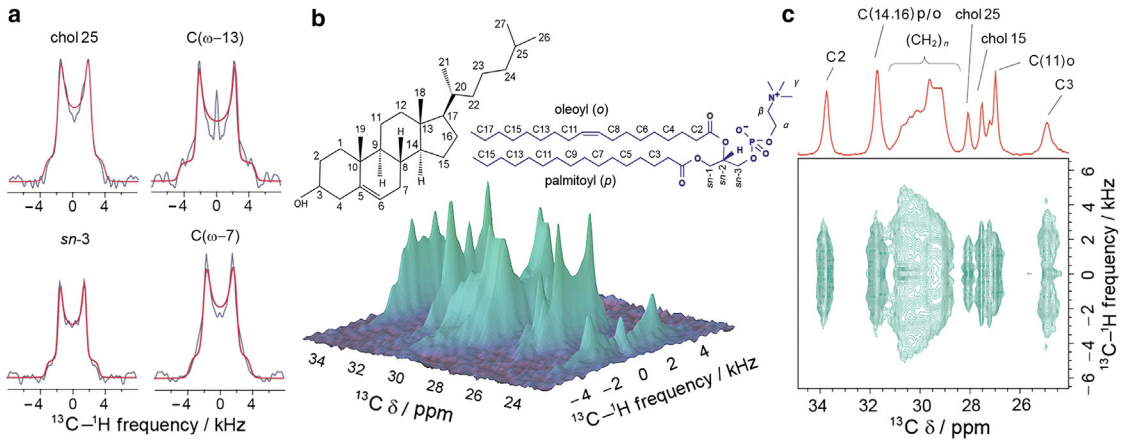

FIGURE 1 Site-specific ^{13}C–^{1}H RDCs are measured using a 2D DROSS spectrum for the case of the POPC/cholesterol (1:1) binary mixture at 30°C. (*a*) Selected recoupled powder patterns showing experimental (*gray*) and simulated (*red*) lineshapes. (*b*) Oblique view of the aliphatic fingerprint region of the DROSS spectrum of the binary system POPC/cholesterol. (*c*) A 2D plane of the spectrum shown in *b*. The ^{13}C isotropic chemical shift (δ) spectrum is shown along F_2 (the horizontal axis) (*red*). The peak separation of the Pake doublet yields the site-specific ^{13}C-^{1}H dipolar coupling along F_1 (the vertical axis). Segmental $|S_{CH}|$ order parameter values are calculated as a function of peak position according to Eq. 2. To see this figure in color, go online.

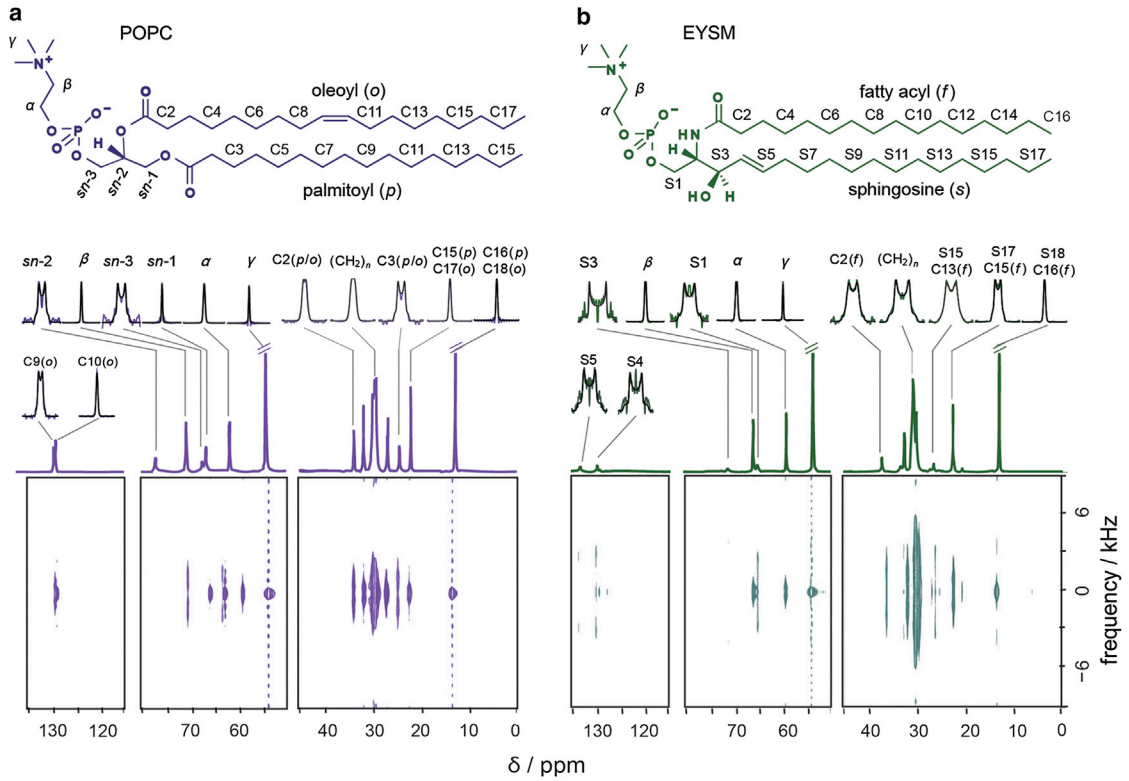

FIGURE 2 SLF ^{13}C NMR spectroscopy of membrane lipids provides site-specific RDCs in the liquid-crystalline phase. 2D DROSS spectra show isotropic chemical-shift projections in the F_2 (horizontal) dimension and ^{1}H-^{13}C dipolar couplings in the F_1 (vertical) dimension for POPC at 28°C (*a*) and EYSM at 48°C (*b*). The Pake lineshapes corresponding to the dipolar splitting for each carbon chemical-shift position are shown above the isotropic chemical-shift spectra. To see this figure in color, go online.

rules reported for isotropic liquids (61,62,64,65). Even so, in the spectral region between 29.5 ppm and 31.5 ppm there is considerable overlap of the resonances from lipid hydrocarbon chain segments.

Because literature chemical shifts are unavailable for individual carbons in this spectral region, initially we assigned those resonance peaks solely depending on ^{13}C chemical shifts of isotropic liquids. For each of the resolved peaks, the spectra obtained for the F_1 dimension were fit with Pake lineshapes to extract site-specific RDC values along the hydrocarbon chains, as well as for the lipid backbone and choline headgroup regions. The ^{1}H-^{13}C order parameter values were calculated according to Eq. 2. Results for the calculated $|S_{CH}|$ order parameters were then compared with the corresponding solid-state ^{2}H-NMR-derived $|S_{CD}|$ values. Both the $|S_{CH}|$ and $|S_{CD}|$ order parameters were consistent for those segmental positions having well-defined ^{13}C chemical-shift assignments. However, in the region between 29.5 ppm and 31.5 ppm, we observed a discrepancy between the $|S_{CH}|$ and $|S_{CD}|$ order parameters for the DMPC bilayer at 30°C (Figs. S5 and S6). The discrepancies are more pronounced in the case of POPC lipid bilayers, where overlapping resonances from the palmitoyl and oleoyl hydrocarbon chains further complicate the peak assignments.

Chemical-shift assignments of MAS carbon-13 NMR spectra

With MAS, the ^{13}C chemical shifts of lipid bilayers are not averaged to liquid-phase isotopic chemical shifts. Instead, they correspond to the chemical-shift values averaged over the molecular conformations present in the liquid-crystalline phase. By contrast, the NMR chemical shifts for a particular site (i) in the solution state $\delta_{iso}^{(i)}$ are averaged over all possible conformations because of the rapid molecular rotations and rotational isomerizations about the chemical bonds. Similar observations in proteins and polypeptides indicate that the ^{13}C chemical shifts strongly depend on the average molecular conformation (88). The observed chemical shifts $\delta_{obs}^{(i)}$ under MAS can be expressed for a given segment position as $\delta_{obs}^{(i)} = \delta_{iso}^{(i)} + \Delta\delta^{(i)}$. The secondary chemical-shift values $\Delta\delta^{(i)}$ are indicative of the molecular structures. For polymers, proteins, and polypeptides, a statistical analysis of $\Delta\delta^{(i)}$ values provides an intrinsic probe for conformational characterization and secondary structure determination (88–90). An in-depth analysis of conformation-dependent chemical shifts in the case presented here requires theoretical calculations based on molecular orbital theory (91,92), which is beyond the scope of this work. One strategy for assigning the isotropic ^{13}C

NMR chemical shifts entails selective ^{2}H isotopic labeling, leading to suppression of cross-polarization from the abundant ^{1}H nuclei (45). An alternative entails comparison of the dipolar order parameters to the quadrupolar order parameters measured in ^{2}H NMR spectroscopy, which we propose as a means of $|S_{CD}|$-assisted ^{13}C NMR spectral assignments.

In this work, we implemented the $|S_{CD}|$-assisted ^{13}C resonance assignments (see Figs. S6–S8) by making use of available ^{2}H solid-state NMR data (43). The resulting $|S_{CH}|$ order profiles as a function of carbon position are shown in Fig. 3 for DMPC, POPC, and EYSM bilayers in the liquid-crystalline (also known as the liquid-disordered (l_d)) state. The absolute order profiles show a decreasing trend as the peak (carbon) index (i) changes from the headgroup to the acyl chain methyl end. Tethering of the acyl chains to the aqueous interface results in order parameters that are higher near the headgroups than near the methyl ends of the acyl chain (93). In the case of ^{13}C NMR for DMPC and EYSM (Fig. 3, *a* and *d*), the order parameters for the individual acyl chains were not separately identified. However, ^{13}C NMR for POPC (Fig. 3, *b* and *c*) shows that the unsaturated carbons (C9 and C10) and allylic carbons (C8 and C11), as well as additional carbon positions from the *sn*-2 acyl chain, were distinct from the *sn*-1 chain ^{13}C resonances. It follows that separate order profiles were determined for the palmitoyl and oleoyl chains (Fig. 3, *b* and *c*). Comparison of the dipolar $|S_{CH}|$ order parameters to the quadrupolar $|S_{CD}|$ order parameters is given in Figs. S7 and S8 for POPC in the l_d phase. For EYSM, assignments of the chemical shifts to the sphingosine backbone carbon positions were limited to the C1, C3, C4, and C5 sites. The C2 position was not observed, due either to line broadening caused by quadrupolar coupling to the ^{14}N nucleus or to its close chemical-shift proximity to the intense γ choline methyl position.

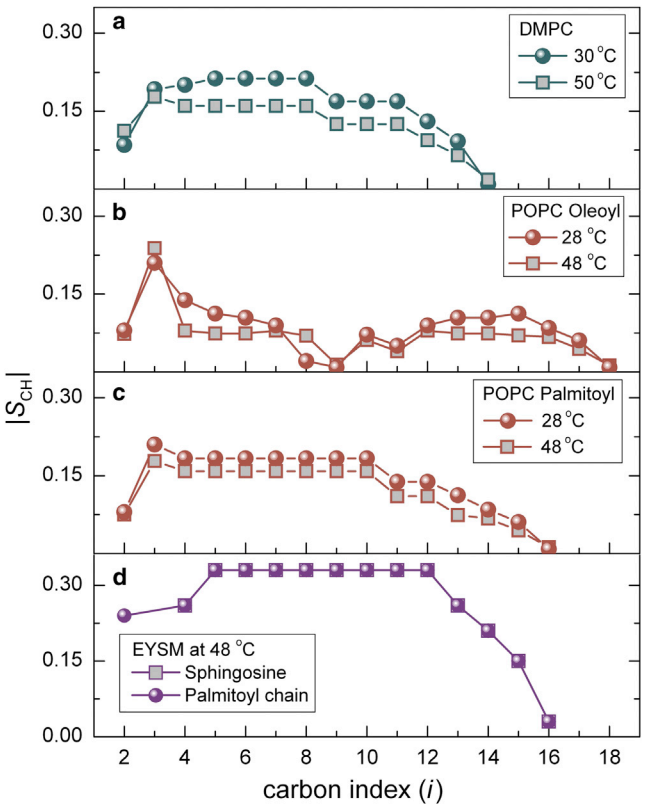

FIGURE 3 Segmental $|S_{CH}|$ order parameters are derived from SLF ^{13}C NMR spectroscopy for lipid bilayers in the l_d phase. Absolute order profiles are plotted with magnitude decreasing as a function of peak (carbon) index (i). Results are shown for DMPC (*a*), the *sn*-2 oleoyl chain of POPC (*b*), the *sn*-1 palmitoyl chain of POPC (*c*), and the sphingosine and palmitoyl chains of EYSM (*d*). Order parameters for the individual chains are not separately presented for DMPC and EYSM. See individual profiles for symbol codes. Relatively high order parameters for the EYSM sphingosine and palmitoyl chains indicate that it is less flexible than the other lipids in the liquid-crystalline (l_d) state. The $|S_{CH}|$ order parameters represent the ^{13}C-^{1}H bond orientational distributions with respect to the membrane normal and are used to calculate the area per lipid within the bilayer. To see this figure in color, go online.

The above findings show that solid-state ^{13}C NMR at natural abundance is complementary to ^{2}H NMR spectroscopy of membrane lipid bilayers (50). Bilayer structural properties including the volumetric hydrocarbon thickness and area per lipid can be obtained without the need for ^{2}H-labeling, which can be time-consuming, expensive, and otherwise prohibitive (see below). The ^{13}C chemical-shift assignments, together with the dipolar couplings and segmental order parameters, are summarized in Tables S1–S5. Fig. 4 shows a comparison between the DROSS-derived $|S_{CH}|$ and $|S_{CD}|$ values for DMPC. For the DMPC bilayer at 50°C, in the liquid-crystalline (l_d) state, the nearly unit slope for the plot of $|S_{CD}|$ versus $|S_{CH}|$ (Fig. 4, *a* and *b*) indicates the consistence of both the ^{2}H solid-state NMR and ^{13}C SLF NMR results in calculating the lipid segmental order parameters. The $|S_{CD}|$-assisted assignments of the solid-state ^{13}C NMR chemical shifts lead to dipolar $|S_{CH}|$ order parameters that are generally in good agreement with the results of corresponding ^{2}H NMR experiments (35). However, the dynamic timescales that average out these interactions are dissimilar, owing to the difference between the rigid-lattice coupling constants (40.7 kHz for ^{13}C nuclei and 167 kHz for ^{2}H nuclei) (60,94). For DMPC at 30°C and for POPC, there are some additional deviations that could be due either to misassignment of some of the peaks or to different motional scalings of the lineshapes that may require future investigation (Figs. S5, S7, and S8).

Cholesterol-containing lipid bilayers in the l_o phase

One striking feature we consider in this work is the drastic increase of absolute order parameters for acyl chain segments of liquid-ordered (l_o) bilayers containing cholesterol versus l_d bilayers (95). Here, it is possible that the cholesterol may exert its effects through either the chains, the headgroup, or possibly both regions of the lipids. To better

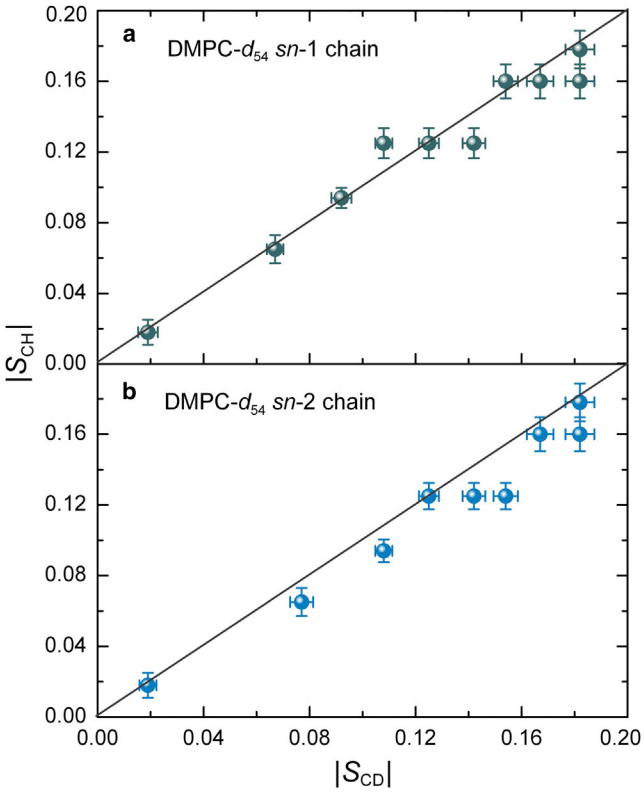

FIGURE 4 SLF ^{13}C NMR spectroscopy gives segmental $|S_{CH}|$ order parameters that agree with ^{2}H solid-state NMR-derived $|S_{CD}|$ order parameters. Data are shown for the *sn*-1 (*a*) and *sn*-2 (*b*) chains of DMPC-d_{54} at 50°C in the liquid-crystalline (l_d) phase. The solid line represents a unit slope. Data for the C2 segment position are not included because of the different order parameters for the initial segment of the acyl chain. The error bars correspond to the standard deviations in the measured RDCs in multiple DROSS experiments. To see this figure in color, go online.

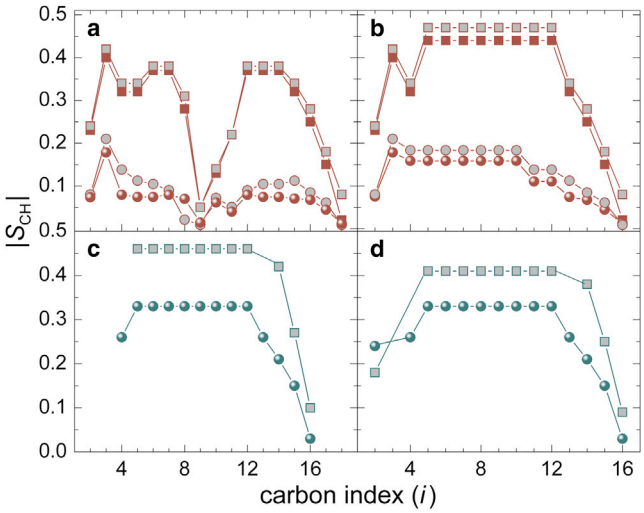

FIGURE 5 Segmental order parameter $|S_{CH}|$ profiles from SLF ^{13}C NMR spectroscopy indicate a lipid-specific loss of conformational disorder due to cholesterol. Order profiles are plotted in terms of decreasing absolute magnitude for the *sn*-2 oleoyl chain of POPC (*a*), the *sn*-1 palmitoyl chain of POPC (*b*), the *sn*-2 sphingosine chain of EYSM (*c*), and the *sn*-1 palmitoyl chain of EYSM (*d*). Circles represent pure lipids and squares represent lipid mixtures with cholesterol (1:1). For POPC, data are shown at two temperatures, 28°C (*gray-filled symbols*) and 48°C (*solid symbols*), and for EYSM at 48°C. Note that upon adding cholesterol the $|S_{CH}|$ order parameters increase more in POPC than in EYSM. To see this figure in color, go online.

understand the structural perturbations indicated by the RDCs, we performed DROSS experiments on POPC and EYSM bilayers in the l_o phase containing 50 mol % cholesterol. Using the INEPT polarization transfer for liquid-crystalline samples, chemically shifted resonances are prominent for the distal alkyl chain positions because of the effective magnetization transfer. For relatively immobile molecular regions with large static dipolar couplings, several sterol ring positions are detected by Hartmann-Hahn cross-polarization techniques (96,97) that helped in assigning many positions of the sterol ring and alkyl chain chemical shifts of cholesterol (54). In general, the RDC lineshape quality is limited by the signal/noise ratio afforded by the chemically shifted resonances.

Representative order-parameter profiles showing the influence of cholesterol for the l_o phases of POPC and EYSM are provided in Fig. 5. The higher magnitudes of $|S_{CH}|$ values for both lipid bilayers at various carbon positions are an indication of the l_o phase (8,98–101) due to interaction with cholesterol (95,102,103). The nonequivalence of the segments of the *sn*-1 and *sn*-2 chains observed in ^{2}H solid-state NMR experiments (104) is clearly reflected in the case of POPC (Fig. 5, *a* and *b*). There is a decreasing trend in $|S_{CH}|$ from the upper acyl positions toward the distal end of the chain. At the uppermost acyl sites (C2 segment of oleoyl and palmitoyl chains), an initial downturn effect corresponds to RDCs that are reduced compared with nearest-neighbor carbon positions. In addition, monounsaturation of the oleoyl chain at the C9 and C10 sites renders the two vinyl ^{13}C-^{1}H positions orientationally nonequivalent both to each other and to the other saturated chain segments (104). The terminal methyl groups of the acyl chains exhibit a very small RDC because of the reorientation and threefold symmetry of the methyl ^{13}C-^{1}H bonds. For EYSM, most notable are the $|S_{CH}|$ values associated with the sphingosine backbone sites (Fig. 5, *c* and *d*). The largest couplings of these sites are observed at the upper C3 position, which may participate in interfacial exchange-type C3-OH hydrogen bonding and/or in C3-OH acceptor and NH donor hydrogen bonding. The large value is suggestive of a static backbone orientation assisted by hydrogen-bonding in the l_d phase and stabilized through lipid packing.

DISCUSSION

Separated local-field spectroscopy (45–47) at natural ^{13}C abundance expands the range of applications of solid-state NMR in membrane biophysics in significant new ways. The development and use of biophysical methods for

biomembranes can benefit by extending the ^{2}H NMR approach (50) to cases where ^{2}H-isotope labeling is impractical. Sphingolipids and other natural lipids can be investigated, together with their interactions both with cholesterol in raftlike lipid mixtures and with membrane proteins. It has been proposed that in complexes with cholesterol and/or receptor proteins, sphingolipids form functional microdomains in putative lipid rafts (9,19,105,106). Such membrane lipids in the brain and other organs are associated with second-messenger events implicated in intracellular signaling and cholesterol shuttling (23,107,108). Applications of solid-state ^{13}C NMR methods to polyunsaturated lipid bilayers (72,109) have also been described. In these examples and others, we are interested in the relationship between molecular properties of membrane lipids and their biological functions within the broader context of structural biophysics (1,5,6,11).

^{13}C-^{1}H dipolar couplings allow calculations of lipid bilayer structure

The DROSS experimental method (46) allows measurement of the direct ^{13}C-^{1}H dipolar couplings in liquid-crystalline systems, such as lipid bilayers at natural isotopic abundance. Through-space direct ^{13}C-^{1}H dipolar interactions report on the orientation of the individual ^{13}C-^{1}H bonds with respect to the bilayer normal, and they are mathematically isomorphous to the C-^{2}H bond order parameters measured by ^{2}H solid-state NMR spectroscopy. Moreover, unlike ^{2}H solid-state NMR, this technique makes it possible to obtain the average orientation of C-H bond segments without isotopic labeling. Analogous studies have also been performed using switched-angle spinning and off-MAS experiments (110). However, DROSS has multiple advantages over the other experiments mentioned here. For instance, implementation of DROSS does not require specialized hardware to control the orientation of the rotor during the experiment. Another advantage is the ability of DROSS to define the sign of the dipolar coupling with a single set of scaling factors (46). The experiment takes advantage of the larger chemical-shift dispersion of the ^{13}C nucleus that enables assignment to be made to specific carbon atoms. Despite these advantages, however, the DROSS experiment for lipid membranes suffers from significant ^{13}C signal superposition, thus limiting the precision of peak assignments and measurement of assigned order parameters. On the other hand, ω–3 polyunsaturated lipid acyl groups show better resolution of ^{13}C chemical shifts (111), so that DROSS can be conveniently applied as shown by Gawrisch and co-workers (47).

Dipolar order parameters reflect structural and dynamic features of phospholipids and sphingolipids

These studies aim at determining the membrane structural parameters using the largest absolute order parameter as typical of the lipid segments near the headgroup. Because DROSS can determine these order parameters unambiguously, it is a suitable technique for such structural studies. The DROSS experiment enables the order parameters to be assigned to specific carbon atoms in the l_d phase at natural isotopic abundance (see Fig. 1). In the case of the disaturated lipid DMPC, there is significant overlap of ^{13}C resonances from the middle of the hydrocarbon chain, yet we could resolve four to five peaks for eight of the carbons (C4–C11). Detailed assignments are not available for this crowded spectral region. First, we assigned these peaks by calculating the chemical shifts using the additivity rules proposed for isotropic liquids (61–65). With such assignments, the measured $|S_{CH}|$ order parameters for DMPC lipids agreed well with solid-state ^{2}H-NMR-determined $|S_{CD}|$ values (43,112). The overlapped methylene carbon resonances around 30.5 ppm are also incompletely resolved in ^{2}H NMR, and lead to a plateau region in the order profile. A similar assignment strategy did not work for POPC, as the signals from saturated and unsaturated acyl chains significantly overlap. However, by comparing the absolute $|S_{CH}|$ order parameters with ^{2}H-NMR-derived $|S_{CD}|$ order parameters, we could identify the carbon chemical-shift positions. For POPC, the carbon resonances of the unsaturated region (C9 and C10) and the immediately adjacent allylic carbons (C8 and C11) were clearly identified. The order parameter values for the unambiguously identified carbon positions of the palmitoyl and oleoyl chains were consistent with the corresponding $|S_{CD}|$ values. The lower order parameter values for the unsaturated carbon positions compare favorably with those from ^{2}H NMR and MD simulations (93). Notably, EYSM showed higher order parameters than the other lipid bilayers studied, indicating its lower flexibility in the single-component bilayer. Complete peak assignments were not essential for the structural parameter calculations. Thus, the highest order parameter shown by the acyl segments, which corresponds to the plateau value of the ^{2}H NMR order profile, was chosen for structural calculations.

The mean-torque model explains ordering of sphingolipids versus phospholipids

Next, we used dipolar ^{13}C-^{1}H order parameters in combination with the mean-torque model (35) to determine the average cross-sectional area per lipid, $\langle A \rangle$, and volumetric hydrocarbon chain thickness, D_C, of the DMPC bilayer in the l_d phase, and for POPC and EYSM in both the l_d and l_o phases. This structural model has previously been used successfully with ^{2}H NMR order parameters (35,74,113). To avoid complications from chain upturns, the largest dipolar order parameters are used for solid-state ^{13}C NMR; these values correspond to the plateau value used in treating the ^{2}H NMR data. Comparison of the bilayer structural parameters from ^{13}C NMR shows good agreement with the corresponding ^{2}H NMR data (Fig. 4). Referring to

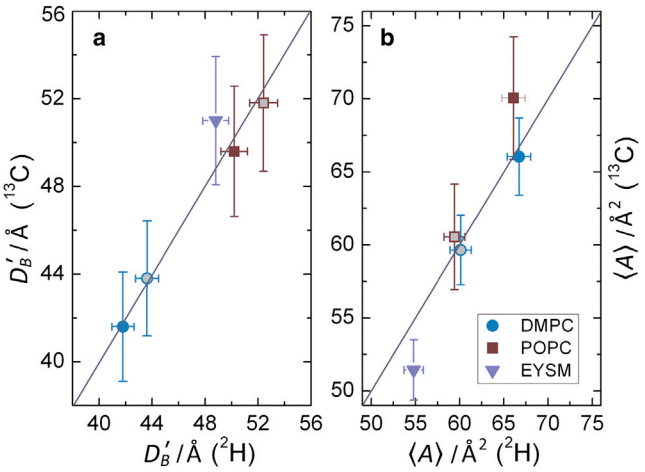

FIGURE 6 Bilayer structural parameters obtained from SLF ^{13}C NMR spectroscopy agree with results from solid-state ^{2}H NMR spectroscopy of lipids that have perdeuterated acyl groups. Parameter values obtained using ^{2}H solid-state NMR are compared with those obtained using the SLF ^{13}C NMR experiment DROSS for bilayer thickness, D_B' (*a*), and area per lipid, $\langle A \rangle$ (*b*). For DMPC and POPC bilayers, structural data are shown at temperatures of 30°C (*solid circles*) and 50°C (*gray-filled circles*), and at 28°C (*squares*) and 48°C (*gray-filled squares*), respectively. Cross-sectional lipid areas are calculated using the plateau $|S_{CD}|$ value in the case of ^{2}H NMR and the highest $|S_{CH}|$ value of the acyl segments in the case of ^{13}C NMR spectroscopy. The unit slope indicates excellent agreement of the two methods. Note that isotopic labeling is not required in the case of solid-state ^{13}C NMR spectroscopy. The estimated error bars correspond to the standard deviations in the measured RDCs in multiple DROSS experiments. To see this figure in color, go online.

Fig. 6, for DMPC in excess water at 30°C, we find an average cross-sectional area per lipid of $\langle A \rangle = 59.5$ Å^2. Note that this value compares favorably to those found using x-ray scattering and ^{2}H solid-state NMR spectroscopy (83). Such agreement for the canonical DMPC bilayer allows us to extend this technique to additional lipid bilayer systems. The main structural results for the different samples are summarized in Table 1. For POPC, we obtain an area per lipid, $\langle A \rangle$, of 70.5 Å^2 at 48°C. By including contributions from the lipid polar headgroups of ≈9 Å/monolayer leaflet (83,84), according to Eq. 4 we arrive at an effective POPC bilayer thickness of $D_B' \approx 46.6$ Å at 48°C. Note that the choice of 9 Å corresponds to the steric bilayer thickness as defined by Nagle et al. (12). In the study described here, we found that EYSM exhibits a strikingly smaller area per lipid of $\langle A \rangle = 51.5$ Å^2 at 48°C. This value is significantly larger than the reported x-ray values but close to the complementary ^{2}H NMR result of 54.8 Å^2 (8). The total bilayer thickness calculated was $D_B' = 49.0$ Å, which compares favorably with both small-angle x-ray measures (114) and ^{2}H NMR values (8). The discrepancy between the ^{13}C-^{1}H and x-ray cross-sectional areas likely reflects the assumptions implicit in the determination of the areas from electron densities (12). Fig. 6, *a* and *b*, compares the structural measurements $\langle A \rangle$ and D_B' in the l_d phases of DMPC, POPC, and EYSM lipid bilayers determined using the different techniques. A nearly unit slope for the plots of solid-state ^{13}C versus ^{2}H NMR-derived values is a clear indication of the consistence of these two techniques in determining lipid structural parameters.

Configurational entropy governs mixing of sphingolipids and phospholipids with cholesterol

Solid-state ^{2}H NMR spectroscopy (85,115) has previously established an umbrellalike model for cholesterol-phospholipid interactions, where the cholesterol C3-OH group is situated beneath the phospholipid headgroups, so that it acts as a spacer molecule as originally proposed by Brown and Seelig (85). Thermodynamically, the cholesterol interactions with DMPC, POPC, and/or EYSM membranes are driven by the hydrophobic effect plus van der Waals interactions between the acyl chains and sterol ring system, giving an l_o phase beyond a threshold cholesterol concentration (116–118). Cholesterol is found to significantly increase

TABLE 1 Structural parameters for lipid bilayers obtained from solid-state ^{13}C and ^{2}H NMR spectroscopy

Lipid	T (°C)	D_C (Å)[a]		D_B' (Å)[a]		⟨A⟩ (Å^2)[a]	
		^{13}C	^{2}H	^{13}C	^{2}H	^{13}C	^{2}H
DMPC	30	12.9 ± 0.5	12.8 ± 0.3	43.8 ± 2.6	43.6 ± 0.9	59.5 ± 3.6	60.0 ± 1.2
	50	11.4 ± 0.4	11.9 ± 0.2	41.6 ± 2.5	41.8 ± 0.8	68.2 ± 4.0	66.1 ± 1.3
POPC	28	14.8 ± 0.6[b]	13.6 ± 0.3[b]	51.8 ± 3.1	52.4 ± 1.1	60.4 ± 3.6	59.3 ± 1.2
		16.7 ± 0.7[c]	15.3 ± 0.4[c]				
	48	12.8 ± 0.5[b]	14.2 ± 0.3[b]	46.6 ± 2.8	50.2 ± 1.0	70.5 ± 4.2	66.2 ± 1.3
		14.4 ± 0.6[c]	16.0 ± 0.3[c]				
EYSM	48	17.5 ± 0.7[b]	16.5 ± 0.4	51.0 ± 3.1	48.8 ± 1.0	51.5 ± 2.1	54.9 ± 1.1
		17.0 ± 0.7[c]	—				
POPC/Cholesterol (1:1)	48	17.8 ± 0.7	—	57.8 ± 3.5	—	45.1 ± 0.9	—
		19.4 ± 0.8	—				
EYSM/Cholesterol (1:1)	48	17.5 ± 0.7	—	53.5 ± 3.2	—	45.5 ± 2.7	—
		18.0 ± 0.7	—				

[a]Error bars correspond to the standard deviations propagated from multiple experimental measurements of RDCs.
[b]*sn*-1 hydrocarbon chain.
[c]*sn*-2 hydrocarbon chain.

the hydrocarbon thickness of the POPC bilayer. Such large volumetric thicknesses are characteristic of both the POPC and EYSM l_o phases. The average bilayer thicknesses for cholesterol-enriched l_o phases are $D_B' \approx 56.8$ Å and 50.0 Å for POPC and EYSM, respectively. The average cross-sectional areas in the l_o phase are reduced owing to the condensing effect of cholesterol, as discussed by McConnell and co-workers (119). For POPC bilayers containing cholesterol (1:1) we find that $\langle A \rangle = 45.1$ Å^2, and for EYSM, $\langle A \rangle = 45.5$ Å^2 at 48°C (Table 1). The cholesterol ordering effect on lipid bilayer stiffening is limited by the maximum acyl length. Furthermore, membranes comprising EYSM/cholesterol may be affected by sphingosine backbone hydrogen bonding and packing interfacial hydrogen bonding involving the NH donor and cholesterol C3-OH acceptor. Such interactions are observed in MD simulations (120,121), although supporting experimental evidence remains elusive (122–127). Another observation is that the sphingosine backbone possesses both an OH hydrogen-bond acceptor and an NH hydrogen-bond donor, which may lead to interlipid hydrogen-bonding and possibly to super-lattice formation in the l_d phase (128).

Readers should note that the cholesterol-mediated structural perturbations are clearly less pronounced for the sphingolipid EYSM than for POPC in the l_o phase. Upon addition of 50 wt % cholesterol, the increase in absolute segmental order parameters is $\approx$0.25 for POPC and $\approx$0.12 for EYSM, as indicated in Fig. 5, *b* and *c* (comparisons are for the maximum $|S_{CH}|$ values due to the plateau region of the order profiles). Correspondingly, the increase in the hydrocarbon thickness and condensation of area per lipid is less for EYSM than for POPC bilayers. Such a remarkable difference indicates that EYSM is in a relatively ordered state in the single-component membrane. The higher acyl segmental order parameters in single-component bilayers at a given temperature for EYSM relative to POPC indicates the high propensity of self-association for the hydrophobic moieties of sphingomyelin lipids (9,27). Notably, these observations suggest that the entropic loss upon adding cholesterol is less pronounced for EYSM than for POPC. A greater loss of conformational entropy for POPC versus EYSM may explain selective enrichment of sphingomyelin in putative raftlike microdomains. Mixing of cholesterol is more favorable for sphingolipids compared to phosphatidylcholines, potentially driving the formation of lipid rafts in multicomponent biomembranes (129–131). That is to say, like dissolves like—as we learn in our introductory chemistry courses.

CONCLUSIONS

Natural-abundance ^{13}C separated local-field NMR together with a mean-torque model gives lipid structural parameters that are complementary to those from solid-state ^{2}H NMR spectroscopy. The ^{13}C-^{1}H residual dipolar couplings of membrane lipids were successfully used to calculate the area per lipid and bilayer thickness. Differences in molecular interactions are resolved by site-specific ^{13}C chemical shifts and $|S_{CH}|$ dipolar order parameters, giving insight into interfacial molecular packing and hydrophobic interactions. The behavior of glycerophospholipids and sphingolipids in the l_d and l_o phases reflects the balance of compositional heterogeneity and chemical structure in biological systems. Despite a common thermodynamic l_o phase for both lipids, their molecular interactions with cholesterol vary significantly. The higher order of EYSM lipids versus POPC lipids implies that the entropy loss due to interactions with cholesterol is less, favoring the association of EYSM over POPC in raftlike lipid mixtures. Moreover, SLF NMR experiments can address key membrane lipid roles of polyunsaturated lipid bilayers and lipid mixtures containing biologically active peptides or proteins. An important question for future research is how the average material properties emerge from the atomic-level interactions in lipid bilayers as investigated by solid-state NMR spectroscopy and related biophysical methods.

SUPPORTING MATERIAL

Eight figures, five tables, and supporting methods are available at http://www.biophysj.org/biophysj/supplemental/S0006-3495(14)00789-9.

This article is dedicated to Professor Harden McConnell.

Support of this research by the National Institutes of Health and by the Arizona Biomedical Research Commission is gratefully acknowledged.

SUPPORTING CITATIONS

Reference (132) appears in the Supporting Material.

REFERENCES

1. Brown, M. F. 2012. Curvature forces in membrane lipid-protein interactions. *Biochemistry.* 51:9782–9795.
2. Gibson, N. J., and M. F. Brown. 1993. Lipid headgroup and acyl chain composition modulate the MI-MII equilibrium of rhodopsin in recombinant membranes. *Biochemistry.* 32:2438–2454.
3. Brown, M. F. 1997. Influence of non-lamellar forming lipids on rhodopsin. *In* Lipid Polymorphism and Membrane Properties. R. Epand, editor. Academic Press, New York, pp. 285–356.
4. Simons, K., and D. Toomre. 2000. Lipid rafts and signal transduction. *Nat. Rev. Mol. Cell Biol.* 1:31–39.
5. Lee, A. G. 2004. How lipids affect the activities of integral membrane proteins. *Biochim. Biophys. Acta.* 1666:62–87.
6. Phillips, R., T. Ursell, …, P. Sens. 2009. Emerging roles for lipids in shaping membrane-protein function. *Nature.* 459:379–385.
7. Botelho, A. V., N. J. Gibson, …, M. F. Brown. 2002. Conformational energetics of rhodopsin modulated by nonlamellar-forming lipids. *Biochemistry.* 41:6354–6368.
8. Bartels, T., R. S. Lankalapalli, …, M. F. Brown. 2008. Raftlike mixtures of sphingomyelin and cholesterol investigated by solid-state ^{2}H NMR spectroscopy. *J. Am. Chem. Soc.* 130:14521–14532.
9. Lingwood, D., and K. Simons. 2010. Lipid rafts as a membrane-organizing principle. *Science.* 327:46–50.

10. Sanders, C. R., and K. F. Mittendorf. 2011. Tolerance to changes in membrane lipid composition as a selected trait of membrane proteins. *Biochemistry.* 50:7858–7867.
11. Soubias, O., and K. Gawrisch. 2012. The role of the lipid matrix for structure and function of the GPCR rhodopsin. *Biochim. Biophys. Acta.* 1818:234–240.
12. Nagle, J. F., and S. Tristram-Nagle. 2000. Structure of lipid bilayers. *Biochim. Biophys. Acta.* 1469:159–195.
13. Gumbart, J., Y. Wang, …, K. Schulten. 2005. Molecular dynamics simulations of proteins in lipid bilayers. *Curr. Opin. Struct. Biol.* 15: 423–431.
14. Botelho, A. V., T. Huber, …, M. F. Brown. 2006. Curvature and hydrophobic forces drive oligomerization and modulate activity of rhodopsin in membranes. *Biophys. J.* 91:4464–4477.
15. Künze, G., P. Barré, …, D. Huster. 2012. Binding of the three-repeat domain of tau to phospholipid membranes induces an aggregated-like state of the protein. *Biochim. Biophys. Acta.* 1818:2302–2313.
16. Teague, Jr., W. E., O. Soubias, …, K. Gawrisch. 2013. Elastic properties of polyunsaturated phosphatidylethanolamines influence rhodopsin function. *Faraday Discuss.* 161:383–395, discussion 419–459.
17. Shevchenko, A., and K. Simons. 2010. Lipidomics: coming to grips with lipid diversity. *Nat. Rev. Mol. Cell Biol.* 11:593–598.
18. Wolf, C., and P. J. Quinn. 2008. Lipidomics in diagnosis of lipidoses. *Subcell. Biochem.* 49:567–588.
19. Leftin, A., C. Job, …, M. F. Brown. 2013. Solid-state ^{13}C NMR reveals annealing of raft-like membranes containing cholesterol by the intrinsically disordered protein α-synuclein. *J. Mol. Biol.* 425: 2973–2987.
20. Block, R. C., E. R. Dorsey, …, I. Shoulson. 2010. Altered cholesterol and fatty acid metabolism in Huntington disease. *J. Clin. Lipidol.* 4:17–23.
21. Scarlata, S. 2002. Regulation of the lateral association of phospholipase Cβ_2 and G protein subunits by lipid rafts. *Biochemistry.* 41:7092–7099.
22. Hong, H., and L. K. Tamm. 2004. Elastic coupling of integral membrane protein stability to lipid bilayer forces. *Proc. Natl. Acad. Sci. USA.* 101:4065–4070.
23. Korade, Z., and A. K. Kenworthy. 2008. Lipid rafts, cholesterol, and the brain. *Neuropharmacology.* 55:1265–1273.
24. Day, C. A., and A. K. Kenworthy. 2009. Tracking microdomain dynamics in cell membranes. *Biochim. Biophys. Acta.* 1788:245–253.
25. Kiessling, V., C. Wan, and L. K. Tamm. 2009. Domain coupling in asymmetric lipid bilayers. *Biochim. Biophys. Acta.* 1788:64–71.
26. Golebiewska, U., and S. Scarlata. 2010. The effect of membrane domains on the G protein-phospholipase Cβ signaling pathway. *Crit. Rev. Biochem. Mol. Biol.* 45:97–105.
27. Simons, K., and M. J. Gerl. 2010. Revitalizing membrane rafts: new tools and insights. *Nat. Rev. Mol. Cell Biol.* 11:688–699.
28. Hong, M., Y. Zhang, and F. Hu. 2012. Membrane protein structure and dynamics from NMR spectroscopy. *Annu. Rev. Phys. Chem.* 63:1–24.
29. Das, N., D. T. Murray, and T. A. Cross. 2013. Lipid bilayer preparations of membrane proteins for oriented and magic-angle spinning solid-state NMR samples. *Nat. Protoc.* 8:2256–2270.
30. Zhou, H. X., and T. A. Cross. 2013. Influences of membrane mimetic environments on membrane protein structures. *Annu. Rev. Biophys.* 42:361–392.
31. Kinnun, J. J., K. J. Mallikarjunaiah, …, M. F. Brown. 2014. Elastic deformation and area per lipid of membranes: atomistic view from solid-state deuterium NMR spectroscopy. *Biochim. Biophys. Acta.* Published online June 16: 2014. http://dx.doi.org/10.1016/j.bbamem.2014.06.004.
32. Pastor, R. W., R. M. Venable, and S. E. Feller. 2002. Lipid bilayers, NMR relaxation, and computer simulations. *Acc. Chem. Res.* 35: 438–446.
33. Krepkiy, D., M. Mihailescu, …, K. J. Swartz. 2009. Structure and hydration of membranes embedded with voltage-sensing domains. *Nature.* 462:473–479.
34. Leioatts, N., B. Mertz, …, M. F. Brown. 2014. Retinal ligand mobility explains internal hydration and reconciles active rhodopsin structures. *Biochemistry.* 53:376–385.
35. Petrache, H. I., S. W. Dodd, and M. F. Brown. 2000. Area per lipid and acyl length distributions in fluid phosphatidylcholines determined by ^{2}H NMR spectroscopy. *Biophys. J.* 79:3172–3192.
36. Feller, S. E. 2000. Molecular dynamics simulations of lipid bilayers. *Curr. Opin. Colloid Interface Sci.* 5:217–223.
37. Dietrich, C., L. A. Bagatolli, …, E. Gratton. 2001. Lipid rafts reconstituted in model membranes. *Biophys. J.* 80:1417–1428.
38. Tristram-Nagle, S., Y. Liu, …, J. F. Nagle. 2002. Structure of gel phase DMPC determined by x-ray diffraction. *Biophys. J.* 83: 3324–3335.
39. Tristram-Nagle, S., and J. F. Nagle. 2004. Lipid bilayers: thermodynamics, structure, fluctuations, and interactions. *Chem. Phys. Lipids.* 127:3–14.
40. Cegelski, L., C. V. Rice, …, J. Schaefer. 2006. Mapping the locations of estradiol and potent neuroprotective analogues in phospholipid bilayers by REDOR. *Drug Dev. Res.* 66:93–102.
41. Dvinskikh, S. V., V. Castro, and D. Sandström. 2005. Efficient solid-state NMR methods for measuring heteronuclear dipolar couplings in unoriented lipid membrane systems. *Phys. Chem. Chem. Phys.* 7: 607–613.
42. Kučerka, N., J. F. Nagle, …, J. Katsaras. 2008. Lipid bilayer structure determined by the simultaneous analysis of neutron and x-ray scattering data. *Biophys. J.* 95:2356–2367.
43. Leftin, A., and M. F. Brown. 2011. An NMR database for simulations of membrane dynamics. *Biochim. Biophys. Acta.* 1808:818–839.
44. Mallikarjunaiah, K. J., A. Leftin, …, M. F. Brown. 2011. Solid-state ^{2}H NMR shows equivalence of dehydration and osmotic pressures in lipid membrane deformation. *Biophys. J.* 100:98–107.
45. Ferreira, T. M., F. Coreta-Gomes, …, D. Topgaard. 2013. Cholesterol and POPC segmental order parameters in lipid membranes: solid state ^{1}H-^{13}C NMR and MD simulation studies. *Phys. Chem. Chem. Phys.* 15:1976–1989.
46. Gross, J. D., D. E. Warschawski, and R. G. Griffin. 1997. Dipolar recoupling in MAS NMR: a probe for segmental order in lipid bilayers. *J. Am. Chem. Soc.* 119:796–802.
47. Gawrisch, K., N. V. Eldho, and I. V. Polozov. 2002. Novel NMR tools to study structure and dynamics of biomembranes. *Chem. Phys. Lipids.* 116:135–151.
48. Castro, V., B. Stevensson, …, A. Maliniak. 2008. NMR investigations of interactions between anesthetics and lipid bilayers. *Biochim. Biophys. Acta.* 1778:2604–2611.
49. Soberón-Chávez, G., and R. M. Maier. 2011. Biosurfactants: a general overview. *In* Biosurfactants. G. Soberón-Chávez, editor. Springer, Heidelberg, pp. 1–11.
50. Brown, M. F. 1996. Membrane structure and dynamics studied with NMR spectroscopy. *In* Biological Membranes: A Molecular Perspective from Computation and Experiment. K. M. Merz, Jr. and B. Roux, editors. Birkhäuser, Basel, pp. 175–252.
51. Petrache, H. I., and M. F. Brown. 2007. X-ray scattering and solid-state deuterium nuclear magnetic resonance probes of structural fluctuations in lipid membranes. *In* Methods in Molecular Biology. A. M. Dopico, editor. Humana, Totowa, NJ, pp. 341–353.
52. Otten, D., M. F. Brown, and K. Beyer. 2000. Softening of membrane bilayers by detergents elucidated by deuterium NMR spectroscopy. *J. Phys. Chem. B.* 104:12119–12129.
53. Sefcik, M. D., J. Schaefer, …, M. F. Brown. 1983. Lipid bilayer dynamics and rhodopsin-lipid interactions: new approach using high-resolution solid-state ^{13}C NMR. *Biochem. Biophys. Res. Commun.* 114:1048–1055.

54. Brown, M. F., and S. I. Chan. 2007. Bilayer membranes: deuterium & carbon-13 NMR. *In* Encyclopedia of Magnetic Resonance. R. K. Harris and D. M. Grant, editors. John Wiley & Sons, Chichester. Published online: 15 March 2007. http://dx.doi.org/10.1002/9780470034590.emrstm0023.

55. McDermott, A. 2009. Structure and dynamics of membrane proteins by magic angle spinning solid-state NMR. *Annu. Rev. Biophys.* 38: 385–403.

56. Leftin, A., X. Xu, and M. F. Brown. 2014. Phospholipid bilayer membranes: deuterium and carbon-13 NMR spectroscopy. *eMagRes.* In press. http://dx.doi.org/10.1002/9780470034590.emrstm1368.

57. Warschawski, D. E., and P. F. Devaux. 2005. Order parameters of unsaturated phospholipids in membranes and the effect of cholesterol: a ^{1}H-^{13}C solid-state NMR study at natural abundance. *Eur. Biophys. J.* 34:987–996.

58. Tycko, R., G. Dabbagh, and P. A. Mirau. 1989. Determination of chemical shift anisotropy lineshapes in a two dimensional magic angle spinning NMR experiment. *J. Magn. Reson.* 85:265–274.

59. Fung, B. M., A. K. Khitrin, and K. Ermolaev. 2000. An improved broadband decoupling sequence for liquid crystals and solids. *J. Magn. Reson.* 142:97–101.

60. Brown, M. F. 1984. Unified picture for spin-lattice relaxation of lipid bilayers and biomembranes. *J. Chem. Phys.* 80:2832–2836.

61. Fürst, A., and E. Pretsch. 1990. A computer program for the prediction of ^{13}C-NMR chemical shifts of organic compounds. *Anal. Chim. Acta.* 229:17–25.

62. Pretsch, E., A. Fürst, …, M. E. Munk. 1992. C13shift: a computer program for the prediction of ^{13}C NMR spectra based on an open set of additivity rules. *J. Chem. Inf. Comput. Sci.* 32:291–295.

63. Schaller, R. B., and E. Pretsch. 1994. A computer program for the automatic estimation of ^{1}H NMR chemical shifts. *Anal. Chim. Acta.* 290:295–302.

64. Schaller, R. B., C. Arnold, and E. Pretsch. 1995. New parameters for predicting ^{1}H NMR chemical shifts of protons attached to carbon-atoms. *Anal. Chim. Acta.* 312:95–105.

65. Schaller, R. B., M. E. Munk, and E. Pretsch. 1996. Spectra estimation for computer-aided structure determination. *J. Chem. Inf. Comput. Sci.* 36:239–243.

66. Brown, M. F. 1982. Theory of spin-lattice relaxation in lipid bilayers and biological membranes. ^{2}H and ^{14}N quadrupolar relaxation. *J. Chem. Phys.* 77:1576–1599.

67. Nevzorov, A. A., and M. F. Brown. 1997. Dynamics of lipid bilayers from comparative analysis of ^{2}H and ^{13}C nuclear magnetic resonance relaxation data as a function of frequency and temperature. *J. Chem. Phys.* 107:10288–10310.

68. Xu, X., A. V. Struts, and M. F. Brown. 2014. Generalized model-free analysis of nuclear spin relaxation experiments. *eMagRes.* In press. http://dx.doi.org/10.1002/9780470034590.emrstm1367.

69. Brown, M. F., J. Seelig, and U. Häberlen. 1979. Structural dynamics in phospholipid bilayers from deuterium spin-lattice relaxation time measurements. *J. Chem. Phys.* 70:5045–5053.

70. Nagle, J. F. 1993. Area/lipid of bilayers from NMR. *Biophys. J.* 64:1476–1481.

71. Seelig, A., and J. Seelig. 1974. The dynamic structure of fatty acyl chains in a phospholipid bilayer measured by deuterium magnetic resonance. *Biochemistry.* 13:4839–4845.

72. Salmon, A., S. W. Dodd, …, M. F. Brown. 1987. Configurational statistics of acyl chains in polyunsaturated lipid bilayers from ^{2}H NMR. *J. Am. Chem. Soc.* 109:2600–2609.

73. Koenig, B. W., H. H. Strey, and K. Gawrisch. 1997. Membrane lateral compressibility determined by NMR and x-ray diffraction: effect of acyl chain polyunsaturation. *Biophys. J.* 73:1954–1966.

74. Petrache, H. I., K. Tu, and J. F. Nagle. 1999. Analysis of simulated NMR order parameters for lipid bilayer structure determination. *Biophys. J.* 76:2479–2487.

75. Dill, K. A., and P. J. Flory. 1980. Interphases of chain molecules: monolayers and lipid bilayer membranes. *Proc. Natl. Acad. Sci. USA.* 77:3115–3119.

76. Dill, K. A., and P. J. Flory. 1981. Molecular organization in micelles and vesicles. *Proc. Natl. Acad. Sci. USA.* 78:676–680.

77. Brown, M. F., A. A. Ribeiro, and G. D. Williams. 1983. New view of lipid bilayer dynamics from ^{2}H and ^{13}C NMR relaxation time measurements. *Proc. Natl. Acad. Sci. USA.* 80:4325–4329.

78. Nagle, J. F., and D. A. Wilkinson. 1978. Lecithin bilayers. Density measurement and molecular interactions. *Biophys. J.* 23:159–175.

79. Jansson, M., R. L. Thurmond, …, M. F. Brown. 1992. Deuterium NMR study of intermolecular interactions in lamellar phases containing palmitoyllysophosphatidylcholine. *J. Phys. Chem.* 96:9532–9544.

80. Petrache, H. I., S. E. Feller, and J. F. Nagle. 1997. Determination of component volumes of lipid bilayers from simulations. *Biophys. J.* 72:2237–2242.

81. Armen, R. S., O. D. Uitto, and S. E. Feller. 1998. Phospholipid component volumes: determination and application to bilayer structure calculations. *Biophys. J.* 75:734–744.

82. Maulik, P. R., D. Atkinson, and G. G. Shipley. 1986. X-ray scattering of vesicles of *N*-acyl sphingomyelins. Determination of bilayer thickness. *Biophys. J.* 50:1071–1077.

83. Petrache, H. I., S. Tristram-Nagle, and J. F. Nagle. 1998. Fluid phase structure of EPC and DMPC bilayers. *Chem. Phys. Lipids.* 95:83–94.

84. Kučerka, N., S. Tristram-Nagle, and J. F. Nagle. 2005. Structure of fully hydrated fluid phase lipid bilayers with monounsaturated chains. *J. Membr. Biol.* 208:193–202.

85. Brown, M. F., and J. Seelig. 1978. Influence of cholesterol on the polar region of phosphatidylcholine and phosphatidylethanolamine bilayers. *Biochemistry.* 17:381–384.

86. Sears, B. 1975. ^{13}C nuclear magnetic resonance studies of egg phosphatidylcholine. *J. Membr. Biol.* 20:59–73.

87. Volke, F., R. Waschipky, …, P. Welzel. 1997. Characterisation of antibiotic moenomycin A interaction with phospholipid model membranes. *Chem. Phys. Lipids.* 85:115–123.

88. Baldus, M. 2002. Correlation experiments for assignment and structure elucidation of immobilized polypeptides under magic angle spinning. *Prog. Nucl. Magn. Reson. Spectrosc.* 41:1–47.

89. Saitô, H., I. Ando, and A. Ramamoorthy. 2010. Chemical shift tensor - the heart of NMR: insights into biological aspects of proteins. *Prog. Nucl. Magn. Reson. Spectrosc.* 57:181–228.

90. Ando, I. 2012. Some aspects of the NMR chemical shift/structure correlation in the structural characterization of polymers and biopolymers. *Polym. J.* 44:734–747.

91. Kondo, M., I. Ando, …, A. Nishioka. 1976. Theoretical calculation of carbon-13 NMR shielding constants and their tensors in hydrocarbons by finite perturbation method. *J. Magn. Reson.* 24:315–326.

92. Ando, I., H. Saitô, …, T. Ozaki. 1984. Conformation-dependent ^{13}C NMR chemical shifts of poly(L-alanine) in the solid state: FPT INDO calculation of *N*-acetyl-*N*′-methyl-L-alanine amide as a model compound of poly(L-alanine). *Macromolecules.* 17:457–461.

93. Huber, T., K. Rajamoorthi, …, M. F. Brown. 2002. Structure of docosahexaenoic acid-containing phospholipid bilayers as studied by ^{2}H NMR and molecular dynamics simulations. *J. Am. Chem. Soc.* 124: 298–309.

94. Brown, M. F. 1984. Theory of spin-lattice relaxation in lipid bilayers and biological membranes. Dipolar relaxation. *J. Chem. Phys.* 80:2808–2831.

95. Ipsen, J. H., O. G. Mouritsen, and M. Bloom. 1990. Relationships between lipid membrane area, hydrophobic thickness, and acyl-chain orientational order. The effects of cholesterol. *Biophys. J.* 57: 405–412.

96. Forbes, J., C. Husted, and E. Oldfield. 1988. High-field, high-resolution proton "magic-angle" sample-spinning nuclear magnetic resonance spectroscopic studies of gel and liquid crystalline lipid

bilayers and the effects of cholesterol. *J. Am. Chem. Soc.* 110:1059–1065.

97. Holland, G. P., and T. M. Alam. 2006. Multi-dimensional ^{1}H-^{13}C HETCOR and FSLG-HETCOR NMR study of sphingomyelin bilayers containing cholesterol in the gel and liquid crystalline states. *J. Magn. Reson.* 181:316–326.
98. Martinez, G. V., E. M. Dykstra, …, M. F. Brown. 2002. NMR elastometry of fluid membranes in the mesoscopic regime. *Phys. Rev. E.* 66:0509021-1–0509021-4.
99. Martinez, G. V., E. M. Dykstra, …, M. F. Brown. 2004. Lanosterol and cholesterol-induced variations in bilayer elasticity probed by ^{2}H NMR relaxation. *Langmuir.* 20:1043–1046.
100. Warschawski, D. E., and P. F. Devaux. 2005. ^{1}H-^{13}C polarization transfer in membranes: a tool for probing lipid dynamics and the effect of cholesterol. *J. Magn. Reson.* 177:166–171.
101. Lai, A. L., and J. H. Freed. 2014. HIV gp41 fusion peptide increases membrane ordering in a cholesterol-dependent fashion. *Biophys. J.* 106:172–181.
102. Chen, Z., and R. P. Rand. 1997. The influence of cholesterol on phospholipid membrane curvature and bending elasticity. *Biophys. J.* 73:267–276.
103. Filippov, A., G. Orädd, and G. Lindblom. 2003. The effect of cholesterol on the lateral diffusion of phospholipids in oriented bilayers. *Biophys. J.* 84:3079–3086.
104. Seelig, J., and A. Seelig. 1980. Lipid conformation in model membranes and biological membranes. *Q. Rev. Biophys.* 13:19–61.
105. Kaiser, H.-J., D. Lingwood, …, K. Simons. 2009. Order of lipid phases in model and plasma membranes. *Proc. Natl. Acad. Sci. USA.* 106:16645–16650.
106. Quinn, P. J. 2013. Structure of sphingomyelin bilayers and complexes with cholesterol forming membrane rafts. *Langmuir.* 29:9447–9456.
107. Barenholz, Y., and T. E. Thompson. 1999. Sphingomyelin: biophysical aspects. *Chem. Phys. Lipids.* 102:29–34.
108. Epand, R. M., and R. F. Epand. 2004. Non-raft forming sphingomyelin-cholesterol mixtures. *Chem. Phys. Lipids.* 132:37–46.
109. Wassall, S. R., and W. Stillwell. 2009. Polyunsaturated fatty acid-cholesterol interactions: domain formation in membranes. *Biochim. Biophys. Acta.* 1788:24–32.
110. Hong, M., K. Schmidt-Rohr, and A. Pines. 1995. NMR measurement of signs and magnitudes of C-H dipolar couplings in lecithin. *J. Am. Chem. Soc.* 117:3310–3311.
111. Brown, M. F., A. J. Deese, and E. A. Dratz. 1982. Proton, carbon-13, and phosphorus-31 NMR methods for the investigation of rhodopsin-lipid interactions in retinal rod outer segment membranes. *Methods Enzymol.* 81:709–728.
112. Oldfield, E., M. Meadows, …, R. Jacobs. 1978. Spectroscopic studies of specifically deuterium labeled membrane systems. Nuclear magnetic resonance investigation of the effects of cholesterol in model systems. *Biochemistry.* 17:2727–2740.
113. Petrache, H. I., A. Salmon, and M. F. Brown. 2001. Structural properties of docosahexaenoyl phospholipid bilayers investigated by solid-state ^{2}H NMR spectroscopy. *J. Am. Chem. Soc.* 123:12611–12622.
114. Maulik, P. R., and G. G. Shipley. 1996. *N*-palmitoyl sphingomyelin bilayers: structure and interactions with cholesterol and dipalmitoylphosphatidylcholine. *Biochemistry.* 35:8025–8034.
115. Brown, M. F. 1990. Anisotropic nuclear spin relaxation of cholesterol in phospholipid bilayers. *Mol. Phys.* 71:903–908.
116. Ipsen, J. H., G. Karlström, …, M. J. Zuckermann. 1987. Phase equilibria in the phosphatidylcholine-cholesterol system. *Biochim. Biophys. Acta.* 905:162–172.
117. Tsamaloukas, A., H. Szadkowska, and H. Heerklotz. 2006. Thermodynamic comparison of the interactions of cholesterol with unsaturated phospholipid and sphingomyelins. *Biophys. J.* 90:4479–4487.
118. van Meer, G., D. R. Voelker, and G. W. Feigenson. 2008. Membrane lipids: where they are and how they behave. *Nat. Rev. Mol. Cell Biol.* 9:112–124.
119. McConnell, H. M., and A. Radhakrishnan. 2003. Condensed complexes of cholesterol and phospholipids. *Biochim. Biophys. Acta.* 1610:159–173.
120. Hofsäβ, C., E. Lindahl, and O. Edholm. 2003. Molecular dynamics simulations of phospholipid bilayers with cholesterol. *Biophys. J.* 84:2192–2206.
121. Pandit, S. A., S. Vasudevan, …, H. L. Scott. 2004. Sphingomyelin-cholesterol domains in phospholipid membranes: atomistic simulation. *Biophys. J.* 87:1092–1100.
122. Kan, C.-C., Z.-s. Ruan, and R. Bittman. 1991. Interaction of cholesterol with sphingomyelin in bilayer membranes: evidence that the hydroxy group of sphingomyelin does not modulate the rate of cholesterol exchange between vesicles. *Biochemistry.* 30:7759–7766.
123. Bittman, R., C. R. Kasireddy, …, J. P. Slotte. 1994. Interaction of cholesterol with sphingomyelin in monolayers and vesicles. *Biochemistry.* 33:11776–11781.
124. Slotte, J. P. 1999. Sphingomyelin-cholesterol interactions in biological and model membranes. *Chem. Phys. Lipids.* 102:13–27.
125. Guo, W., V. Kurze, …, J. A. Hamilton. 2002. A solid-state NMR study of phospholipid-cholesterol interactions: sphingomyelin-cholesterol binary systems. *Biophys. J.* 83:1465–1478.
126. Niemelä, P., M. T. Hyvönen, and I. Vattulainen. 2004. Structure and dynamics of sphingomyelin bilayer: insight gained through systematic comparison to phosphatidylcholine. *Biophys. J.* 87:2976–2989.
127. Holopainen, J. M., A. J. Metso, …, P. K. J. Kinnunen. 2004. Evidence for the lack of a specific interaction between cholesterol and sphingomyelin. *Biophys. J.* 86:1510–1520.
128. Somerharju, P., J. A. Virtanen, and K. H. Cheng. 1999. Lateral organisation of membrane lipids. The superlattice view. *Biochim. Biophys. Acta.* 1440:32–48.
129. Ohvo-Rekilä, H., B. Ramstedt, …, J. P. Slotte. 2002. Cholesterol interactions with phospholipids in membranes. *Prog. Lipid Res.* 41:66–97.
130. Edidin, M. 2003. The state of lipid rafts: from model membranes to cells. *Annu. Rev. Biophys. Biomol. Struct.* 32:257–283.
131. Ramstedt, B., and J. P. Slotte. 2006. Sphingolipids and the formation of sterol-enriched ordered membrane domains. *Biochim. Biophys. Acta.* 1758:1945–1956.
132. Shipley, G. G., L. S. Avecilla, and D. M. Small. 1974. Phase behavior and structure of aqueous dispersions of sphingomyelin. *J. Lipid Res.* 15:124–131.

Supporting Material

Area Per Lipid and Cholesterol Interactions in Membranes from Separated Local-Field ^{13}C NMR Spectroscopy

Avigdor Leftin[†,], Trivikram R. Molugu[†], Constantin Job[†], Klaus Beyer[†], and Michael F. Brown[†, ‡,*]

[†]Department of Chemistry and Biochemistry and [‡]Department of Physics, University of Arizona, Tucson, 85721, USA

Separated local-field NMR experiments: The NMR experiment DROSS (dipolar recoupling on-axis with scaling and shape preservation) (1) was implemented with the Bruker Topspin software platform (Billerica, MA). The timing diagram for the pulse sequence is shown in Fig. S1a. Magnetic dipolar recoupling during magic-angle spinning (MAS) is achieved by application of synchronous, phase-shifted recoupling π-pulse blocks (shown in Fig. S1b) during the indirect t_1 dimension. The module preserves the appearance of the Pake powder-pattern lineshapes due to the magnetic dipolar interaction. The conditions for the evolution of the second-rank Hamiltonian under MAS are not unique, and correspond to different values for the scaling of the anisotropic interactions χ_p and ε for the dipolar coupling and chemical shift anisotropy, respectively. For recoupling, we used the four-pulse module described by Tycko et al. (2). By applying symmetric recoupling pulses delivered at rotation angles of ± 70.9º, and ± 110.9º (shown in Fig. S1c), we achieved anisotropy scaling of χ_p = 0.393 and a chemical shift offset of ε = 0. The pulse sequence is sensitive to small errors in the rotor synchronization. Finite pulse widths and internal timing delays of the NMR spectrometer were accounted for in the pulse program. High-power radiofrequency amplifiers included a 1-kW

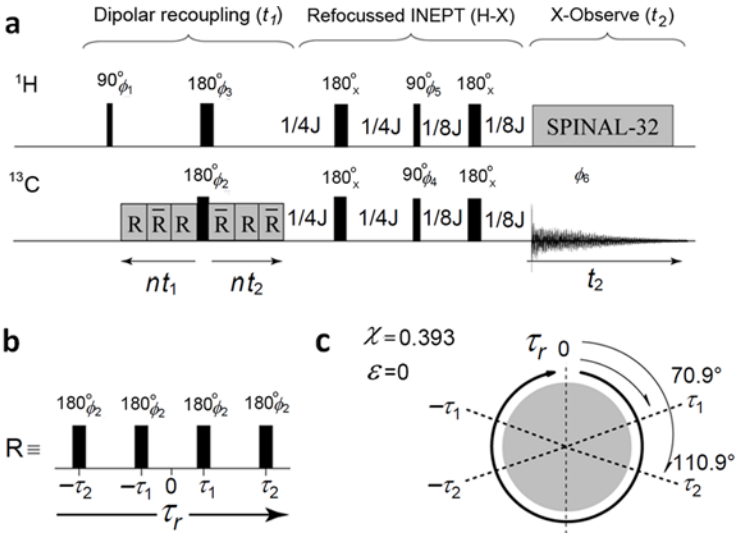

Fig. S1. Schematic representation of pulse sequence for DROSS experiment. (a) Timing diagram, (b) 4-pulse recoupling sequence, and (c) rotor synchronization timing with recoupling parameters χ=0.393 and ε=0.

low-frequency American Microwave Technologies (Lancaster, PA) amplifier and a 500-W high-frequency Tomco Technologies (Adelaide, Australia) amplifier. Radiofrequency pulses for the ^{1}H and ^{13}C channels were adjusted to exactly the same duration of 3.5 μs for the 90º pulses.

The refocused INEPT (insensitive nuclei enhanced by polarization transfer) method transfers dipolar-modulated ^{1}H magnetization to the directly-bound ^{13}C aliphatic nuclei for detection under ^{1}H decoupling using SPINAL-32 (3). The timing of the INEPT module in solution NMR requires $1/4J$ and $1/8J$ delays, with J being the average methylene ^{13}C–^{1}H scalar coupling of $J \approx$ 145 Hz. In the DROSS experiment, under MAS the rotor synchronization of the INEPT transfer, as well as any incompletely averaged dipolar couplings undergoing transverse precession during the polarization step, lead to optimal delays that differ from the solution NMR values. Maximum enhancement was ensured by monitoring the INEPT buildup of anti-phase magnetization and refocusing delays in a pseudo-2D array. For experiments conducted at 8-kHz MAS frequency, these delays were optimized to be 1.72 ms and 0.86 ms.

Two temperatures were chosen to conduct the DROSS experiments, 28 °C and 48 °C. These temperatures were selected based on the solid-ordered (s_o) to liquid-disordered (l_d) phase transition temperature of the EYSM lipid, which is reported to occur at approximately 38 ºC (4). This is an important aspect of our study, because for ^{13}H–^{13}C INEPT polarization transfer to efficiently occur, the components of the lipid membrane must be in the liquid-ordered, liquid-disordered, or isotropic phase (5). The refocused INEPT polarization transfer yields a null spectrum in the solid-ordered (s_o) phase. Hence, our comparisons of lipid mixtures are mostly discussed for results obtained at 48 °C. The behavior of binary membrane systems are qualitatively the same at both 28 ºC and 48 ºC, although magnitudes of the residual dipolar couplings (RDCs) are greater at the lower temperatures, and smaller chemical shift changes are obtained. Temperatures were calibrated to account for frictional and radiofrequency heating of the sample. Phase behavior of the lipids was also checked prior to the ^{13}C NMR experiments by collecting single-pulse ^{1}H NMR spectra. Temperatures reported are accurate to ± 1 ºC.

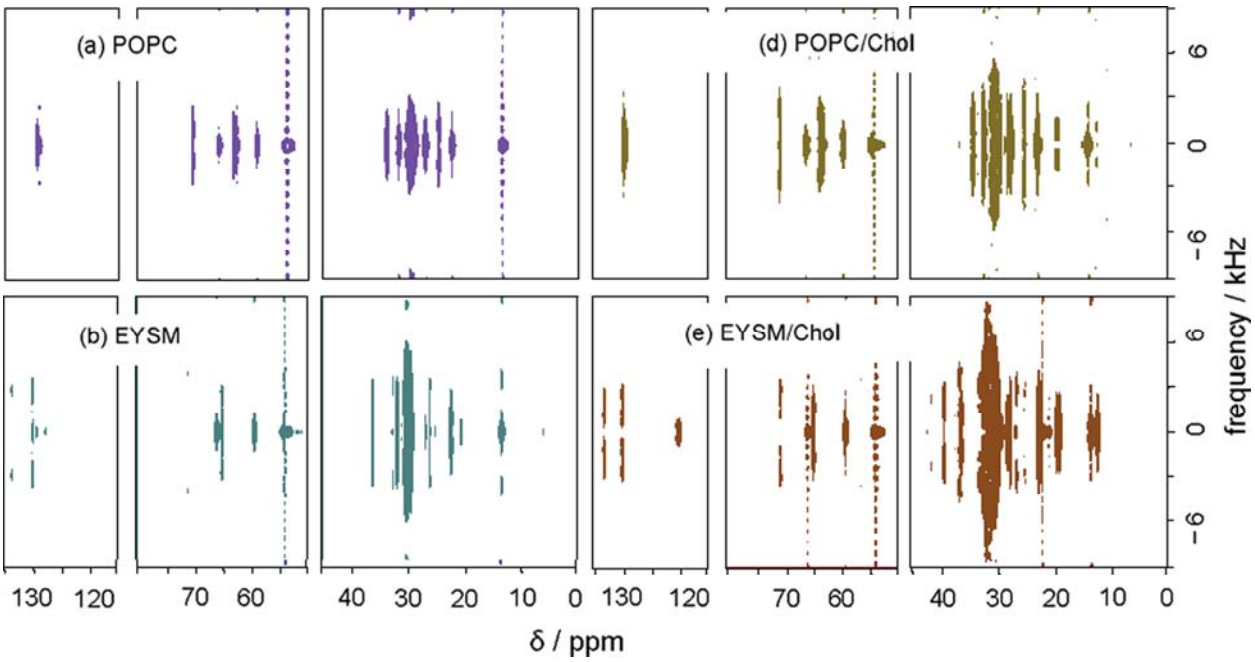

Fig. S2. Two-dimensional ^{13}C–^{1}H separated local-field contour plots for pure lipid bilayers and lipid/ cholesterol mixtures. The 2D planes obtained using the NMR experiment DROSS are shown for (a) POPC, (b) EYSM, (c) POPC/cholesterol (1:1), and (d) EYSM/cholesterol (1:1) lipid bilayers at 48 °C.

We conducted the 2D DROSS experiment for a series of membrane lipid systems to obtain the chemical shifts and RDCs for comparison with the raft-like system. Single-component POPC and EYSM membrane spectra were first collected. Then, the experiments were repeated for two-component POPC/cholesterol (1:1) and EYSM/cholesterol (1:1) bilayers to characterize the spectral behavior of the mixed systems. In Figs. S2a, b we show the separated-local field 2D spectra for the single-component POPC and EYSM membranes, respectively. Corresponding 2D spectra are shown in Figs. S2c, d for POPC/cholesterol (1:1) and EYSM/cholesterol (1:1) lipid mixtures at 48 °C. Isotropic ^{13}C chemical shifts and ^{13}C–^{1}H residual dipolar couplings for the single-component lipid membranes are presented in Fig. S3, and data for binary phospholipid/cholesterol systems in Fig. S4. The spectra demonstrate that the DROSS experiment is sensitive to changes in membrane phase, and that it is possible to extract site-specific ^{13}C chemical shifts and RDCs for individual lipids and lipid/cholesterol mixtures. The ^{13}C chemical shifts, measured ^{1}H–^{13}C residual dipolar couplings, and corresponding segmental order parameters are tabulated in Tables S1–Table S5 for all the samples studied.

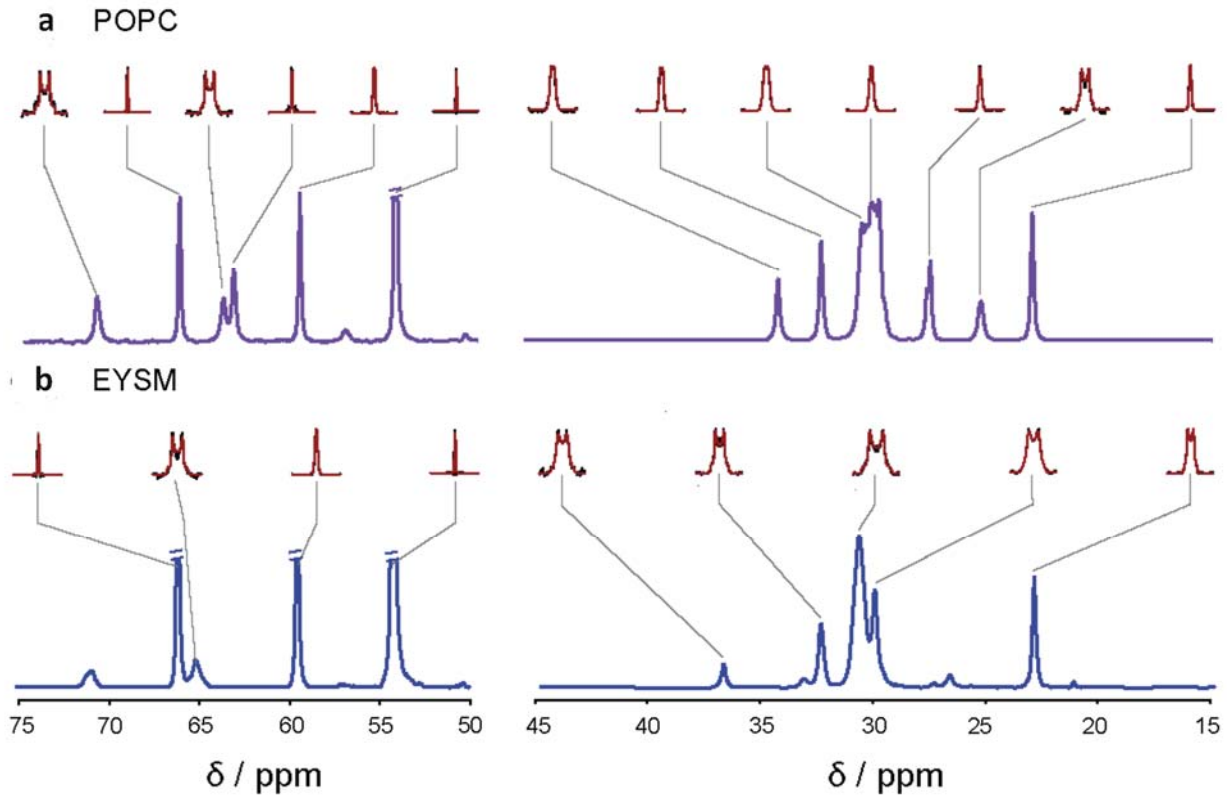

Fig. S3. Separated local-field NMR-derived ^{13}C chemical shifts and ^{13}C–^{1}H residual dipolar couplings (RDCs) for lipid bilayers. The slices along the F_1 (vertical) axis and projections onto the F_2 (horizontal) frequency axis of the 2D contour plots shown in Fig. S2 are indicated for (a) POPC and (b) EYSM (1:1) lipid bilayers at 48 °C.

Chemical shift assignments of solid-state ^{13}C lipid NMR spectra: The ^{13}C isotropic chemical shift spectra obtained under MAS were initially assigned using the literature values (6). However, chemical shift assignments for the region 29.5 ppm to 31.5 ppm are not available, where methylene resonances are significantly overlapping. Initially, we assigned this region using simulations (ChemBioDraw, PerkinElmer, MA) based on additive rules given for isotropic liquids (7-11). Such assignments gave expected results in the case of DMPC bilayers. The $|S_{CH}|$ order parameters were calculated for each chemical shift position and matched well with the $|S_{CD}|$ order parameters (12). For DMPC the ^{1}H–^{13}C dipolar order parameters calculated for the sites identified by such assignments are plotted against the corresponding quadrupolar order parameter values in Figs. S5 and S6 at 30 °C and 50 °C, respectively. For DMPC at 30 °C, a small discrepancy in the observed order parameters is seen for the *sn*-1 (Fig. S5a) and *sn*-2 (Fig. S5b) chains, but at 50 °C such a discrepancy is not seen (Figs. 6a, b).

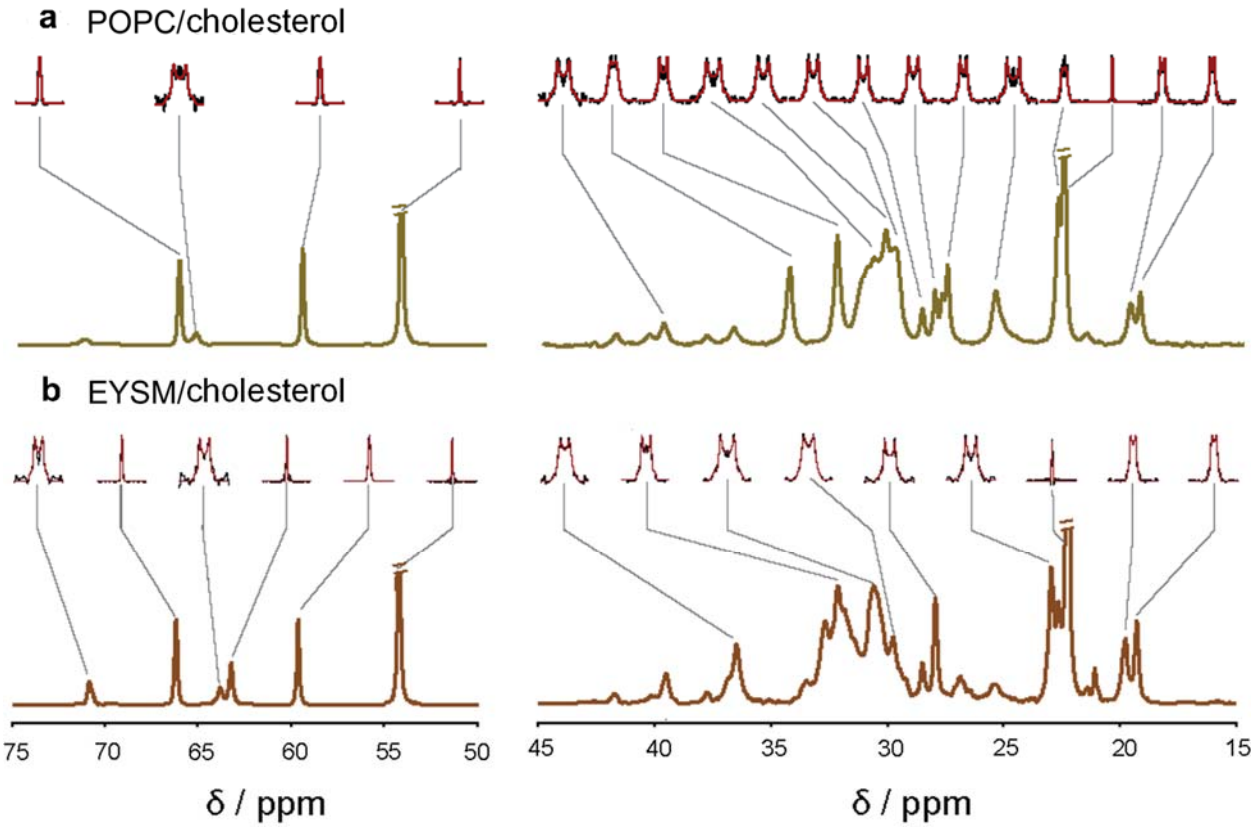

Fig. S4. Experimental ^{13}C chemical shifts and ^{13}C–^{1}H residual dipolar couplings (RDCs) for lipid/cholesterol mixtures. Slices along the F_1 axis (vertical) and F_2 (horizontal) projections of the 2D contour plots shown in Fig. S2 are indicated for (a) POPC/Chol (1:1) and (b) EYSM/Chol (1:1) lipid bilayers at 48 °C.

However, a similar strategy did not give the expected order parameter values in case of POPC bilayers (Figs. S7 and S8). The segmental $|S_{CH}|$ order parameters for unambiguously assigned chemical shift positions still matched with the known $|S_{CD}|$ order parameters (13) (shown as spheres in Figs. 7c, d). Yet the significant overlap of resonance peaks from the *sn*-1 palmitoyl chain and *sn*-2 oleoyl chain complicates the resonance assignments. The MAS-averaged chemical shift tensors of the less flexible acyl groups do not reach the isotropic chemical shift values. Instead they correspond to the chemical shift values due to tensorial averaging over the molecular conformations in the liquid-crystalline phase. At the spin rates employed here (6–8 kHz) MAS averages the residual chemical shielding tensor to its trace, which is not the same as averaging the static chemical shielding tensor. By contrast, in solution state NMR the isotropic chemical shifts are averaged over all possible conformations. Rapid molecular tumbling and rotational isomerizations about the chemical bonds average the static (so-called rigid-lattice) chemical shielding tensor to its isotropic value.

Consequently, we made use of the calculated $|S_{CH}|$ order parameter values at each resolved ^{13}C resonance peak as a basis to assign the ^{13}C chemical shift spectra in the crowded methylene (CH_2) spectral region. Initially the $|S_{CH}|$ order parameter values for all possible chemical shift positions were calculated. The order parameter values for well-defined peaks were then compared with the available $|S_{CD}|$ order parameters (12) at corresponding temperature values. For DMPC the $|S_{CH}|$ and $|S_{CD}|$ values consistently match, as shown by the unit slope in the $|S_{CD}|$ versus $|S_{CH}|$ plots in Figs. S5c, d and Figs. S6c, d. Next, we mapped the remaining calculated order parameters that were unassigned or ambiguously assigned with the known $|S_{CD}|$ order parameters, and fixed the chemical shift positions accordingly. A comparison of the ^2H NMR-assisted assignments and ChemBiodraw-based assignments for POPC bilayers at 28 °C are shown in Fig. S7 for the palmitoyl chain and Fig S8 for the oleoyl acyl chain. In this case the S_{CD}-assisted ^{13}C chemical shift assignments for the palmitoyl *sn*-1 chain (Figs. S7a, c) are in good agreement, whereas there is a significant discrepancy if the ChemBioDraw assignments are used (Figs. S7b, d). In the case of the oleoyl *sn*-2 chain of POPC, the S_{CD}-assisted ^{13}C NMR assignments give better agreement of the $|S_{CH}|$ and $|S_{CD}|$ order parameters (Figs. S8a, c) compared to ChemBioDraw assignments (Figs. S8b, d). Such an assignment strategy may not always apply to resonances that are not well resolved in solid-state ^2H NMR, and are treated as the plateau. Nonetheless, the application of ^2H NMR-assisted assignments is definitely useful for identifying the palmitoyl and oleoyl chains in the present case.

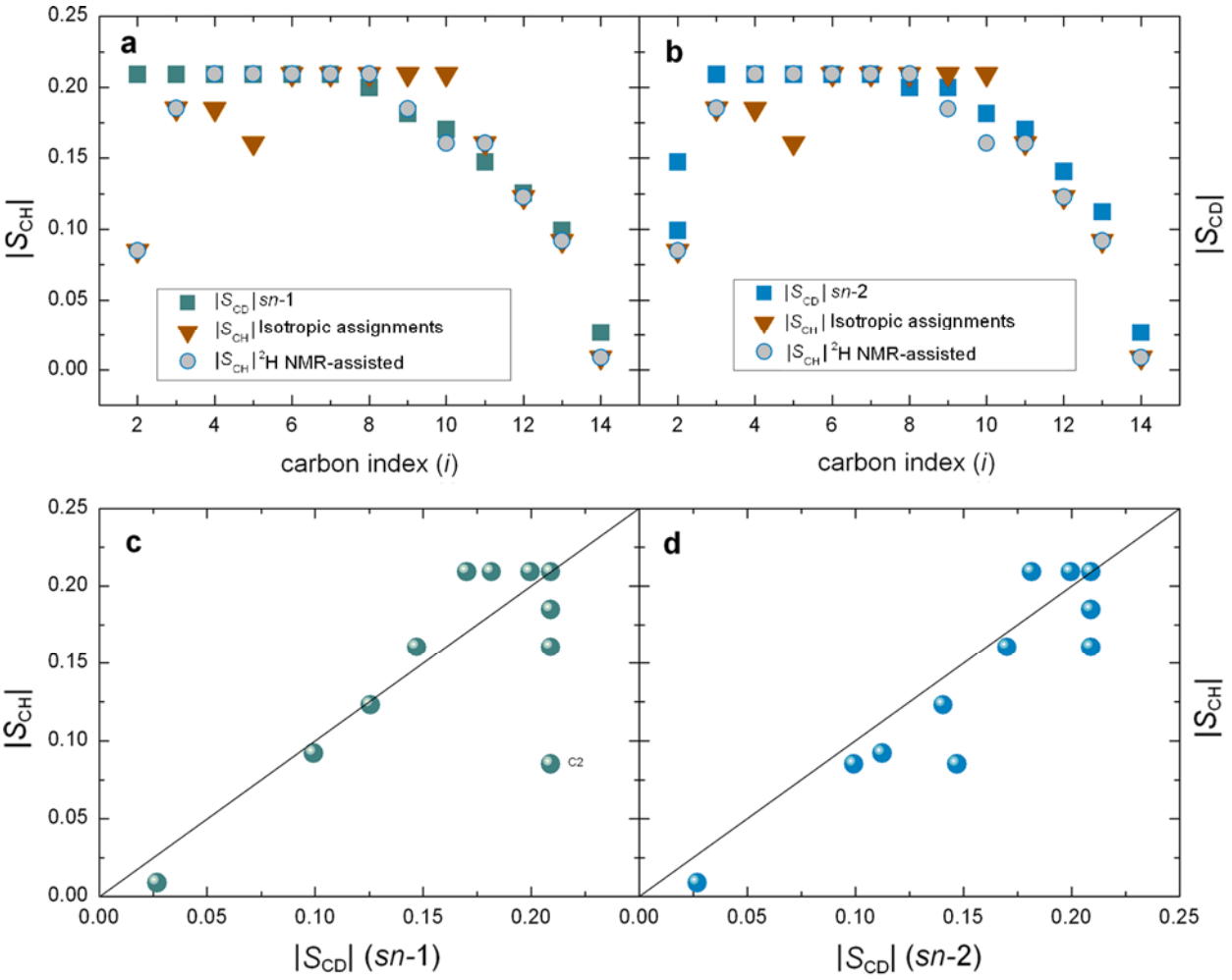

Fig. S5. Separated local-field ^{13}C NMR experiment provides $|S_{CH}|$ order parameters that correspond to $|S_{CD}|$ order parameters for DMPC bilayers in the liquid-crystalline (l_d) state at 30 °C. Absolute order parameters are plotted in terms of decreasing magnitudes as a function of peak (carbon) index (i): (a) $|S_{CD}|$ values (squares), $|S_{CH}|$ values with assignments based on additive rules for isotropic ^{13}C chemical shifts (triangles), and ^{2}H NMR-assisted (circles) order parameters as function of segmental carbon position of *sn*-1 chain. (b) $|S_{CD}|$ values (squares), $|S_{CH}|$ values with isotropic ^{13}C chemical shift assignments (triangles), and ^{2}H NMR-assisted order parameters (circles) as function of segmental carbon position for the *sn*-2 chain. Graphs of $|S_{CH}|$ order parameters from separated local-field ^{13}C NMR versus the corresponding $|S_{CD}|$ order parameters from solid-state ^{2}H NMR spectroscopy: (c) Plot of $|S_{CD}|$ order parameters versus ^{2}H NMR-assisted $|S_{CH}|$ order parameters for *sn*-1 chain. (d) Plot of $|S_{CD}|$ order parameters versus ^{2}H NMR-assisted $|S_{CH}|$ order parameters for *sn*-2 chain. Note that the $|S_{CH}|$ order parameters are in good agreement with the $|S_{CD}|$ values giving a near unit slope. Hence the ^{2}H NMR-derived $|S_{CD}|$ values can be used to guide ambiguous ^{13}C chemical shift assignments.

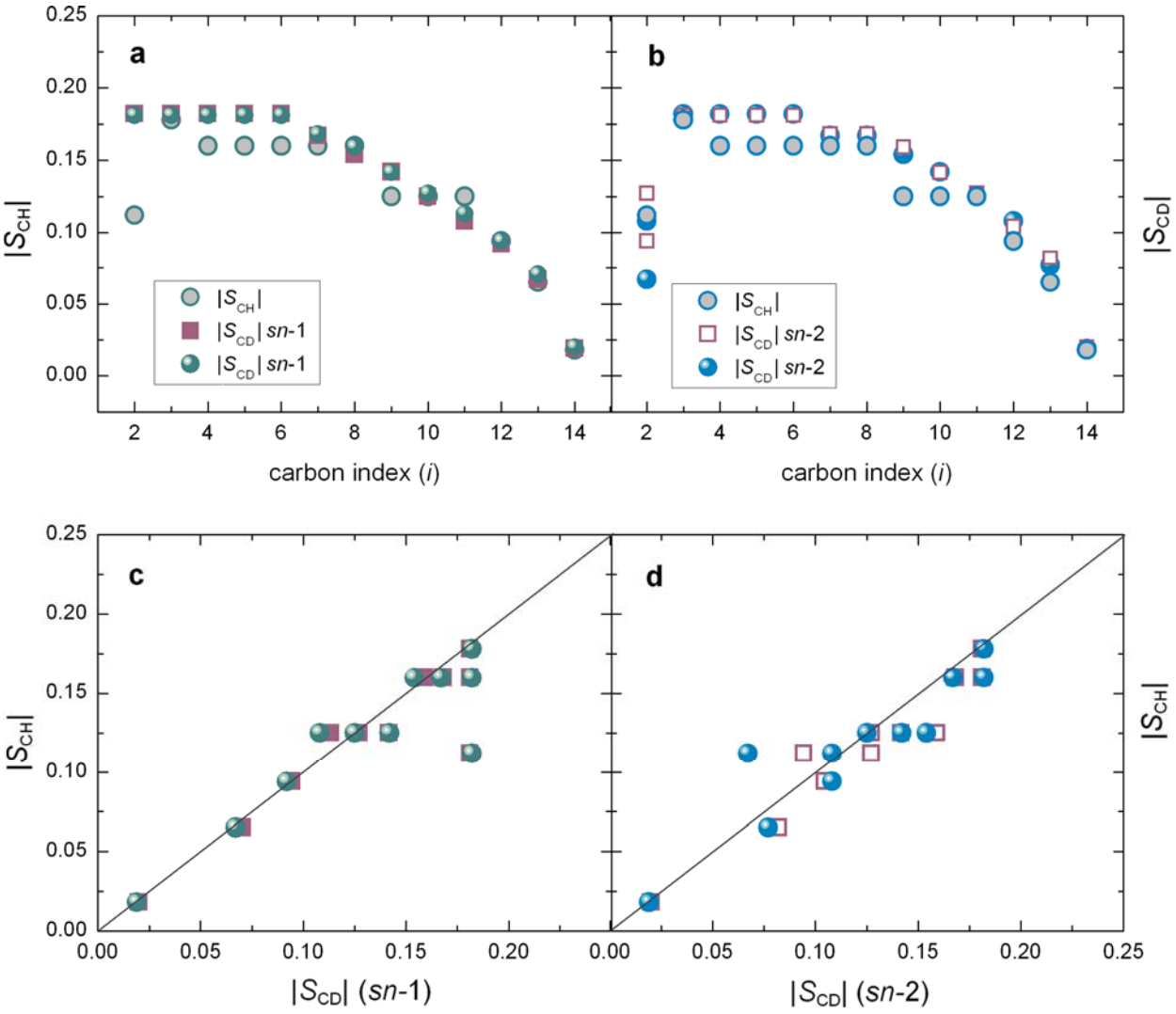

Fig. S6. Comparision of ^{13}C–^{1}H dipolar segmental order parameters $|S_{CH}|$ to corresponding $|S_{CD}|$ order parameters for DMPC bilayers at 50 °C. Absolute order parameters are plotted in terms of decreasing magnitudes as a function of peak (carbon) index (i): (a) $|S_{CH}|$ (grey circles) and $|S_{CD}|$ (spheres and squares) order parameters for *sn*-1 chain, (b) $|S_{CH}|$ (circles), and $|S_{CD}|$ (squares and spheres) order parameters as function of segmental carbon position in *sn*-2 chain. Separated-local field ^{13}C NMR order parameters $|S_{CH}|$ graphed against the $|S_{CD}|$ order parameters from solid-state ^{2}H NMR spectroscopy. (c) Plot of $|S_{CD}|$ order parameters versus $|S_{CH}|$ order parameters for *sn*-1 chain. (d) Plot of $|S_{CD}|$ order parameters versus $|S_{CH}|$ order parameters for *sn*-2 chain. The $|S_{CH}|$ order parameters are in good agreement with the $|S_{CD}|$ values giving a unit slope. In this example, the ^{2}H NMR-assisted method was not needed for ^{13}C chemical shift assignments.

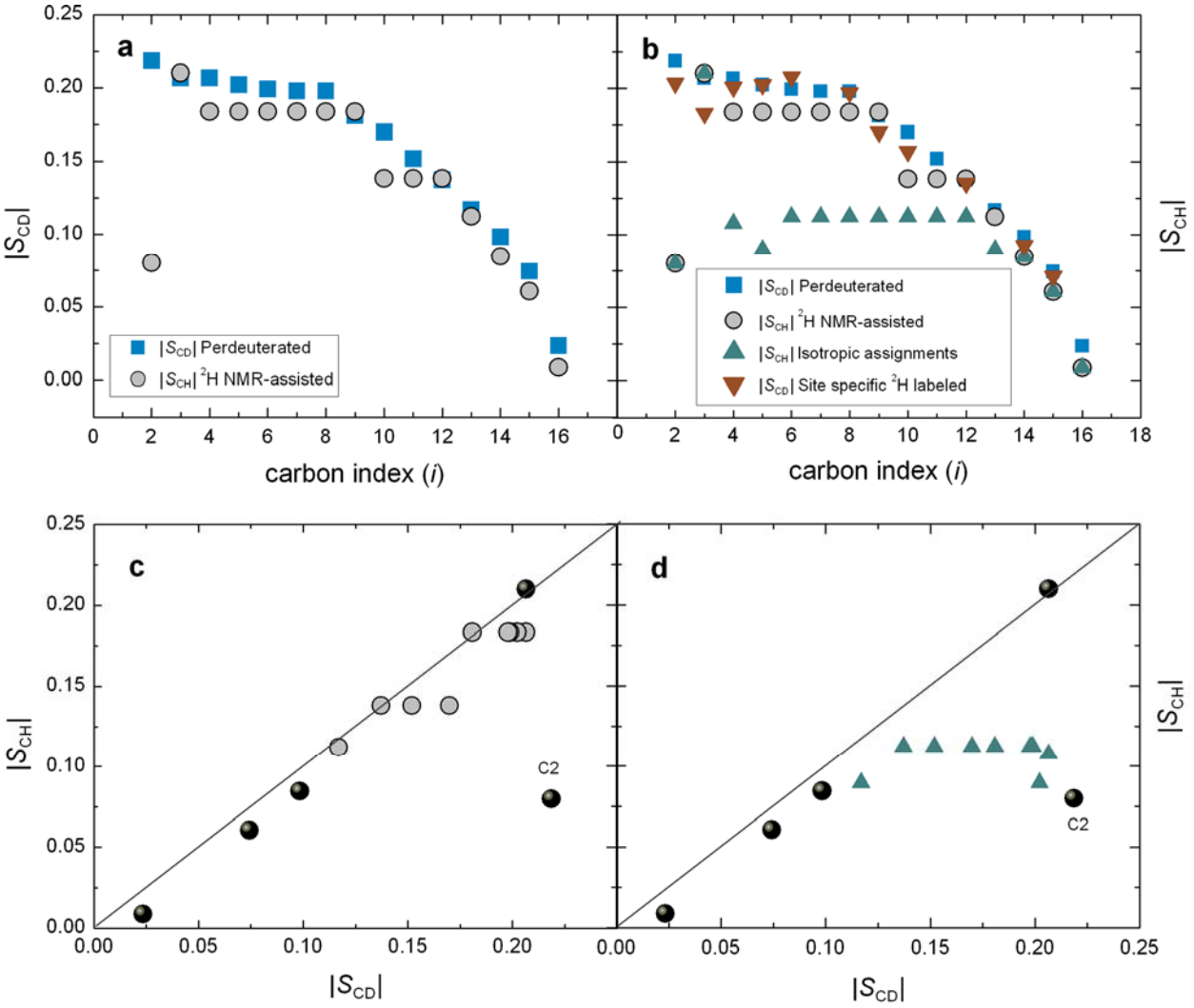

Fig. S7. Comparison of $|S_{CH}|$ order parameters from ^{13}C separated local-field NMR spectroscopy for the *sn*-1 palmitoyl chain of POPC to corresponding $|S_{CD}|$ values allows ^{2}H NMR-assisted chemical shift assignments. The applicability of such an assignment method is illustrated by comparing dipolar and quadrupolar order parameters for the liquid-crystalline (l_d) state of POPC bilayers at 28 °C. (a) The ^{2}H NMR-assisted $|S_{CH}|$ (circles) and $|S_{CD}|$ (squares) order parameters as function of segmental carbon position in the palmitoyl chain. (b) The $|S_{CD}|$ (squares) order parameters measured for the palmitoyl chain of POPC-d_{31} versus ^{2}H NMR-assisted $|S_{CH}|$ values (circles). Graph of the $|S_{CH}|$ order parameters from separated local-field ^{13}C NMR plotted against the corresponding solid-state ^{2}H NMR order parameters. (c) Segmental $|S_{CD}|$ order parameters versus ^{2}H NMR-assisted $|S_{CH}|$ order parameters. (d) $|S_{CD}|$ order parameters of perdeuterated palmitoyl group of POPC-d_{31} versus $|S_{CH}|$ order parameters obtained using isotropic ^{13}C chemical shift assignments. The $|S_{CH}|$ order parameters for all unambiguously assigned carbon positions (spheres in c and d) give a unit slope plotted against the corresponding $|S_{CD}|$ values. Note that ^{2}H NMR-derived $|S_{CD}|$ values can guide ambiguous ^{13}C resonance chemical shift assignments.*

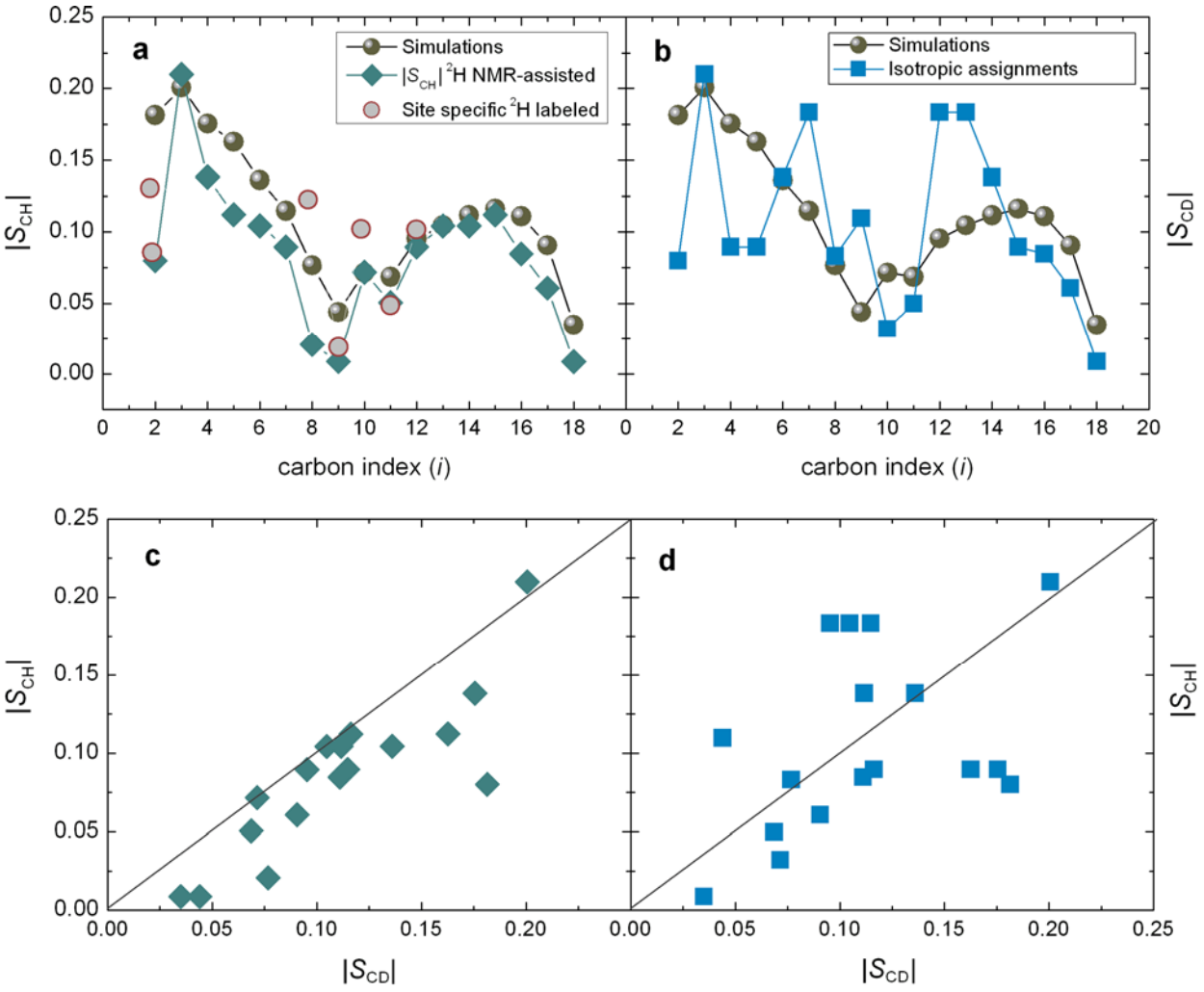

Fig. S8. Application of the $|S_{CD}|$-assisted ^{13}C chemical shift assignment method enables identification of *sn*-2 chain oleoyl resonances in the liquid-crystalline state of POPC at 28 °C. Comparison of $|S_{CH}|$ and $|S_{CD}|$ order parameters for the *sn*-2 oleoyl chain of the POPC lipid bilayer is shown. (a) The $|S_{CH}|$ order parameters with $|S_{CD}|$-assisted ^{13}C resonance assignments (diamonds), $|S_{CD}|$ order parameters (spheres) calculated using molecular dynamics simulations (13), and the $|S_{CD}|$ order parameters determined using ^{2}H-solid-state NMR for site specific deuterated lipid (grey filled circles). (b) The $|S_{CH}|$ order parameters (squares) calculated for *sn*-2 oleoyl chain of POPC with ^{13}C resonance assignments using additivity rules and $|S_{CD}|$ order parameters (spheres) calculated using molecular dynamics simulations. Plot of $|S_{CH}|$ order parameter from separated local-field ^{13}C NMR against the corresponding $|S_{CD}|$ order parameters: (c) Plot of the ^{2}H NMR-assisted $|S_{CH}|$ order parameters versus $|S_{CD}|$ order parameters. (d) The $|S_{CH}|$ order parameters calculated with ChemBioDraw assignments versus $|S_{CD}|$ order parameters.

Table S1. Summary of experimental results for DMPC bilayers

	Chemical Shift[a] / ppm		Dipolar Coupling[b] / Hz		Segmental Order Parameter[c]	
Resonance	30 ºC	50 ºC	30 ºC	50 ºC	30 ºC	50 ºC
C14	14.38	14.26	179.32	175.65	0.01	0.01
C13	23.3	23.15	1422.60	1353.61	0.09	0.08
C12	32.73	32.55	2559.80	1923.66	0.12	0.07
C11	30.32	30.09	3450.38	2541.98	0.12	0.13
C10	30.32	30.59	3450.38	2541.98	0.16	0.13
C9	30.32	30.09	3450.38	2541.98	0.19	0.13
C8	30.87	30.59	3382.19	257500	0.21	0.16
C7	30.87	30.59	3382.19	2575.00	0.21	0.16
C6	30.87	30.59	3382.19	3257.00	0.21	0.16
C5	30.87	30.59	3382.19	2575.00	0.21	0.16
C4	30.32	30.09	3250.38	2541.98	0.21	0.16
C3	30.87	30.59	3982.19	3257.00	0.19	0.18
C2	25.67	25.49	4218.83	3628.5	0.09	0.12
sn-1	64.29	64.24	4920.10	4501.27	0.31	0.29
sn-2	71.33	71.34	2270.74	2064.76	0.14	0.13
sn-3	63.71	63.66	363.87	363.87	0.02	0.02
α	60.11	60.04	280.48	250.53	0.02	0.02
β	66.71	66.73	516.15	368.63	0.03	0.02
γ	54.74	54.74	180.33	200.02	0.01	0.01

[a]Chemical shifts are referenced to TMS (external).

[b]Dipolar couplings are scaled by the pulse sequence scale factor χ_p=0.393.

[c]Absolute value.

Table S2. Summary of experimental results for POPC bilayers

	Chemical Shift[a] / ppm				Dipolar Coupling[b] / Hz				Segmental Order Parameter[c]			
	Palmitoyl		Oleoyl		Palmitoyl		Oleoyl		Palmitoyl		Oleoyl	
Resonance	28 ºC	48 ºC	28 ºC	48 ºC	28 ºC	48 ºC	28 ºC	48 ºC	28 ºC	48 ºC	28 ºC	48 ºC
C18	--	--	13.84	13.78	--	--	323	300	--	--	0.01	0.01
C17	--	--	22.67	22.60	--	--	758	486	--	--	0.06	0.04
C16	13.84	13.78	32.04	31.96	323	300	1120	896	0.01	0.01	0.09	0.07
C15	22.67	22.60	29.75	29.63	758	486	1573	967	0.06	0.04	0.11	0.07
C14	32.04	31.96	29.88	29.82	1120	896	1753	1611	0.09	0.07	0.10	0.07
C13	29.75	29.63	29.88	29.82	1573	967	1753	1611	0.11	0.07	0.10	0.07
C12	29.88	29.82	29.88	29.82	1753	1611	1753	1611	0.14	0.11	0.09	0.08
C11	29.88	29.82	27.25	27.21	1753	1611	725	364	0.14	0.11	0.05	0.04
C10	30.21	30.06	129.34	129.35	1753	1611	486	244	0.18	0.16	0.07	0.06
C9	30.21	30.06	129.72	129.71	1753	1611	1448	1265	0.18	0.16	0.01	0.01
C8	30.21	30.06	27.25	27.21	1753	1611	725	364	0.18	0.16	0.02	0.07
C7	30.21	30.06	29.88	29.82	1753	1611	1753	1611	0.18	0.16	0.09	0.08
C6	30.21	30.06	29.88	29.82	1753	1611	1753	1611	0.18	0.16	0.10	0.07
C5	30.21	30.06	29.75	29.63	1573	967	1573	967	0.18	0.16	0.11	0.07
C4	30.21	30.06	29.47	29.37	1282	364	1282	364	0.18	0.16	0.14	0.08
C3	25.02	24.98	25.02	24.98	2802	2651	2802	2651	0.21	0.18	0.21	0.18
C2	34.07	34.07	34.07	34.07	1552	1448	1552	1448	0.08	0.08	0.08	0.07
sn-1	63.09	63.10	63.09	63.10	244	244	244	244	0.02	0.02	0.02	0.02
sn-2	70.73	70.80	70.73	70.80	2949	2893	2949	2893	0.19	0.18	0.19	0.18
sn-3	63.68	63.66	63.68	63.66	3394	3539	3394	3539	0.21	0.22	0.21	0.22
α	59.50	59.49	59.50	59.49	486	486	486	486	0.03	0.03	0.03	0.03
β	66.11	66.19	66.11	66.19	486	244	486	244	0.03	0.02	0.03	0.02
γ	54.13	54.19	54.13	54.19	303	244	303	244	0.02	0.02	0.02	0.02

[a]Chemical shifts are referenced to TMS (external).

[b]Dipolar couplings are scaled by the pulse sequence scale factor χ_p=0.393.

[c]Absolute value.

Table S3. Summary of experimental results for EYSM bilayers

	Chemical Shift[a] / ppm				Dipolar Coupling[b] / Hz				Segmental Order Parameter[c]			
	Sphingosine		Fatty Acyl		Sphingosine		Fatty Acyl		Sphingosine		Fatty Acyl	
Resonance	28 ºC	48 ºC	28 ºC	48 ºC	28 ºC	48 ºC	28 ºC	48 ºC	28 ºC	48 ºC	28 ºC	48 ºC
C16	--	--	--	14.10	--	--	--	282	--	--	--	0.014
C15	--	--	--	23.07	--	--	--	2249	--	--	--	0.110
S18 / C14	--	14.10	--	32.54	--	282	--	3204	--	0.014	--	0.157
S17 / C13	--	23.07	--	30.15	--	2249	--	3931	--	0.110	--	0.193
S16 / C12	--	32.54	--	30.85	--	3204	--	5064	--	0.157	--	0.248
S15 / C11	--	30.15	--	30.85	--	3931	--	5064	--	0.193	--	0.248
S14 / C10	--	30.85	--	30.85	--	5064	--	5064	--	0.248	--	0.248
S13 / C9	--	30.85	--	30.85	--	5064	--	5064	--	0.248	--	0.248
S12 / C8	--	30.85	--	30.85	--	5064	--	5064	--	0.248	--	0.248
S11 / C7	--	30.85	--	30.85	--	5064	--	5064	--	0.248	--	0.248
S10 / C6	--	30.85	--	30.85	--	5064	--	5064	--	0.248	--	0.248
S9 / C5	--	30.85	--	30.85	--	5064	--	5064	--	0.248	--	0.248
S8 / C4	--	30.85	--	30.15	--	5064	--	3931	--	0.248	--	0.193
S7 / C3	--	30.85	--	26.81	--	5064	--	--	--	0.248	--	--
S6 / C2	--	30.15	--	36.86	--	3931	--	3649	--	0.193	--	0.179
S5	--	134.09	--	--	--	5539	--	--	--	0.272	--	--
S4	--	130.44	--	--	--	5664	--	--	--	0.278	--	--
S3	--	71.57	--	--	--	6837	--	--	--	0.335	--	--
S2	--	--	--	--	--	--	--	--	--	--	--	--
S1	--	65.59	--	65.59	--	4677	--	4677	--	0.229	--	0.229
α	--	59.87	--	59.87	--	282	--	282	--	0.014	--	0.014
β	--	66.48	--	66.48	--	282	--	282	--	0.014	--	0.014
γ	--	54.56	--	54.56	--	282	--	282	--	0.014	--	0.014

[a]Chemical shifts are referenced to TMS (external).

[b]Dipolar couplings are scaled by the pulse sequence scale factor $\chi_p = 0.393$.

[c]Absolute values.

Table S4. Summary of experimental results for POPC/Chol (1:1) bilayers

	Chemical Shift[a] / ppm				Dipolar Coupling[b] / Hz				Segmental Order Parameter[c]			
	Palmitoyl		Oleoyl		Palmitoyl		Oleoyl		Palmitoyl		Oleoyl	
Resonance	28 ºC	48 ºC	28 ºC	48 ºC	28 ºC	48 ºC	28 ºC	48 ºC	28 ºC	48 ºC	28 ºC	48 ºC
C18	--	--	14.12	14.01	--	--	1274	317	--	--	0.08	0.02
C17	--	--	28.57	22.88	--	--	2784	2321	--	--	0.18	0.15
C16	14.12	14.01	32.56	32.41	779	176	4252	3880	0.08	0.02	0.28	0.25
C15	23.02	22.88	30.08	29.93	2753	2321	5237	4845	0.18	0.15	0.34	0.32
C14	32.56	32.41	30.46	30.31	4252	3880	5758	5588	0.28	0.25	0.38	0.37
C13	30.08	29.93	30.46	30.31	5237	4845	5758	5588	0.34	0.32	0.38	0.37
C12	30.46	30.31	31.07	30.82	7262	6768	5758	5588	0.47	0.44	0.38	0.37
C11	30.46	30.31	31.07	30.82	7262	6768	3422	3323	0.47	0.44	0.22	0.22
C10	30.46	30.31	31.07	30.82	7262	6768	2235	2051	0.47	0.44	0.14	0.13
C9	30.46	30.31	31.07	30.82	7262	6768	842	794	0.47	0.44	0.05	0.05
C8	30.46	30.31	31.07	30.82	7262	6768	4669	4344	0.47	0.44	0.31	0.28
C7	30.46	30.31	31.07	30.82	7262	6768	7262	6768	0.47	0.44	0.38	0.37
C6	30.46	30.31	31.07	30.82	7262	6768	5758	5588	0.47	0.44	0.38	0.37
C5	30.46	30.31	31.07	30.82	7262	6768	5237	4845	0.47	0.44	0.34	0.32
C4	30.08	29.93	30.08	29.93	5237	4845	5237	4845	0.34	0.32	0.34	0.32
C3	25.72	25.58	25.72	25.58	6450	6122	6450	6122	0.42	0.40	0.42	0.40
C2	34.50	34.45	34.50	34.45	3608	3537	3608	3537	0.24	0.23	0.24	0.23
sn-1	63.49	63.45	63.49	63.45	349	349	349	349	0.02	0.02	0.02	0.02
sn-2	71.01	71.04	71.01	71.04	4835	4539	4835	4539	0.30	0.29	0.16	0.15
sn-3	64.06	64.01	64.06	64.01	4201	4206	4201	4206	0.27	0.28	0.27	0.28
α	59.84	59.78	59.84	59.78	176	959	176	959	0.01	0.06	0.01	0.06
β	66.41	66.45	66.41	66.45	349	349	349	349	0.02	0.02	0.02	0.02
γ	54.45	54.47	54.45	54.47	344	349	344	349	0.03	0.03	0.03	0.03

[a]Chemical shifts are referenced to TMS (external).

[b]Dipolar couplings are scaled by the pulse sequence scale factor $\chi_p = 0.393$.

[c]Absolute values.

Table S5. Summary of experimental results for EYSM/Chol (1:1) bilayers

	Chemical Shift[a] / ppm				Dipolar Coupling[b] / Hz				Segmental Order Parameter[c]			
	Sphingosine		Fatty Acyl		Sphingosine		Fatty Acyl		Sphingosine		Fatty Acyl	
Resonance	28 ºC	48 ºC	28 ºC	48 ºC	28 ºC	48 ºC	28 ºC	48 ºC	28 ºC	48 ºC	28 ºC	48 ºC
C16	--	--	13.81	13.74	--	--	1041	919	--	--	0.051	0.045
C15	--	--	23.06	22.95	--	--	4092	3761	--	--	0.201	0.184
S18 / C14	13.81	13.74	32.80	32.66	1041	919	6491	5771	0.051	0.045	0.318	0.283
S17 / C13	23.06	22.95	30.84	30.64	4092	3761	6975	6265	0.201	0.184	0.341	0.307
S16 / C12	32.80	32.66	30.84	30.64	6491	5771	6975	6265	0.318	0.283	0.341	0.307
S15 / C11	30.84	30.64	30.84	30.64	6975	6265	6975	6265	0.341	0.307	0.341	0.307
S14 / C10	30.84	30.64	30.84	30.64	6975	6265	6975	6265	0.341	0.307	0.341	0.307
S13 / C9	30.84	30.64	30.84	30.64	6975	6265	6975	6265	0.341	0.307	0.341	0.307
S12 / C8	30.84	30.64	30.84	30.64	6975	6265	6975	6265	0.341	0.307	0.341	0.307
S11 / C7	30.84	30.64	30.84	30.64	6975	6265	6975	6265	0.341	0.307	0.341	0.307
S10 / C6	30.84	30.64	30.84	30.64	6975	6265	6975	6265	0.341	0.307	0.341	0.307
S9 / C5	30.84	30.64	30.84	30.64	6975	6265	6975	6265	0.341	0.307	0.341	0.307
S8 / C4	30.84	30.64	30.84	30.64	6975	6265	6975	6265	0.341	0.307	0.341	0.307
S7 / C3	30.84	30.64	26.97	26.86	6975	6265	--	--	0.341	0.307	--	--
S6 / C2	30.84	30.64	37.03	36.53	6975	6265	--	2687	0.341	0.307	--	0.132
S5	133.59	133.54	133.59	133.54	--	4692	--	4692	--	0.230	--	0.230
S4	130.28	130.31	130.28	130.31	--	4819	--	4819	--	0.236	--	0.236
S3	70.94	70.96	70.94	70.96	5527	5779	5527	5779	0.271	0.283	0.271	0.283
S2	--	--	--	--	--	--	--	--	--	--	--	--
S1	65.09	65.14	65.09	65.14	3705	3550	3705	3550	0.182	0.174	0.182	0.174
α	59.51	59.51	59.51	59.51	244	364	244	364	0.012	0.018	0.012	0.018
β	66.11	66.17	66.11	66.17	318	280	318	280	0.016	0.014	0.016	0.014
γ	54.16	54.22	54.16	54.22	305	244	305	244	0.015	0.012	0.015	0.012

[a]Chemical shifts are referenced to TMS (external).

[b]Dipolar couplings are scaled by the pulse sequence scale factor χ_p=0.393.

[c]Absolute values.

Supporting References

1. Gross, J. D., D. E. Warschawski, and R. G. Griffin. 1997. Dipolar recoupling in MAS NMR: a probe for segmental order in lipid bilayers. *J. Am. Chem. Soc.* 119:796-802.
2. Tycko, R., G. Dabbagh, and P. A. Mirau. 1989. Determination of chemical shift anisotropy lineshapes in a two dimensional magic angle spinning NMR experiment. *J. Magn. Reson.* 85:265-274.
3. Fung, B. M., A. K. Khitrin, and K. Ermolaev. 2000. An improved broadband decoupling sequence for liquid crystals and solids. *J. Magn. Reson.* 142:97-101.
4. Shipley, G. G., L. S. Avecilla, and D. M. Small. 1974. Phase behaviour and structure of aqueous dispersions of sphingomyelin. *J. Lipid Res.* 15:124.
5. Warschawski, D. E., and P. F. Deveaux. 2005. Order parameters of unsaturated phospholipids in membranes and the effect of cholesterol: a ^{1}H-^{13}C solid-state NMR study at natural abundance. *Eur. Biophys. J.* 34:987-996.
6. Volke, F., R. Waschipky, A. Pampel, A. Donnerstag, G. Lantzsch, H. Pfeiffer, W. Richter, G. Klose, and P. Welzel. 1997. Characterisation of antibiotic moenomycin A interaction with phospholipid model membranes. *Chem. Phys. Lipids* 85:115-123.
7. Fürst, A., and E. Pretsch. 1990. A computer program for the prediction of ^{13}C-NMR chemical shifts of organic compounds. *Anal. Chim. Acta* 229:17-25.
8. Pretsch, E., A. Fürst, M. Badertscher, R. Bürgin, and M. E. Munk. 1992. C13shift: a computer program for the prediction of ^{13}C NMR spectra based on an open set of additivity rules. *J. Chem. Inf. Comput. Sci.* 32:291-295.
9. Schaller, R. B., C. Arnold, and E. Pretsch. 1995. New parameters for predicting ^{1}H-NMR chemical-shifts of protons attached to carbon-atoms. *Anal. Chim. Acta* 312:95-105.
10. Schaller, R. B., M. E. Munk, and E. Pretsch. 1996. Spectra estimation for computer-aided structure determination. *J. Chem. Inf. Comput. Sci.* 36:239-243.
11. Schaller, R. B., and E. Pretsch. 1994. A computer-program for the automatic estimation of ^{1}H-NMR chemical-shifts. *Anal. Chim. Acta* 290:295-302.
12. Leftin, A., and M. F. Brown. 2011. An NMR database for simulations of membrane dynamics. *Biochim. Biophys. Acta* 1808:818-839.
13. Huber, T., K. Rajamoorthi, V. F. Kurze, K. Beyer, and M. F. Brown. 2002. Structure of docosahexaenoic acid-containing phospholipid bilayers as studied by ^{2}H NMR and molecular dynamics simulations. *J. Am. Chem. Soc.* 124:298-309.